Polar Biology (2022) 45:1635–1653
https://doi.org/10.1007/s00300-022-03094-5

ORIGINAL PAPER

Control of Antarctic phytoplankton community composition and standing stock by light availability

T. E. G. Biggs[1,2] · P. D. Rozema[3] · C. Evans[4] · K. R. Timmermans[1,3] · M. P. Meredith[5] · D. W. Pond[6] · C. P. D. Brussaard[1,2]

Received: 13 July 2021 / Revised: 3 October 2022 / Accepted: 4 October 2022 / Published online: 19 October 2022

Abstract

Southern Ocean phytoplankton are especially subjected to pronounced seasonal and interannual changes in light availability. Although previous studies have examined the role of light in these environments, very few combined pigment-based taxonomy with flow cytometry to better discriminate the light response of various phytoplankton groups. In particular the different populations within the diverse and important taxonomic group of diatoms require further investigation. Six incubation experiments (9–10 days) were performed during the main productive period with natural seawater collected at the Western Antarctic Peninsula. Standing stock of *Phaeocystis* spp. cells displayed relatively fast accumulation under all levels of light (low, medium, high; 4–7, 30–50 and 150–200 µmol quanta m^{-2} s^{-1}), whilst the small- and larger-sized diatom populations (4.5 and 20 µm diameter) exhibited faster accumulation in medium and high light. In contrast, intermediate-sized diatoms (11.5 µm diameter) displayed fastest net growth under low light, subsequently dominating the phytoplankton community. Low light was a key factor limiting accumulation and peak phytoplankton biomass, except one incubation displaying relatively high accumulation rates under low light. The 3-week low-light period prior to experimentation likely allowed adaptation to maximize achievable growth and seems a strong determinant of whether the different natural Antarctic phytoplankton populations sustain, thrive or decline. Our study provides improved insight into how light intensity modulates the net response of key Antarctic phytoplankton, both between and within taxonomic groups.

Keywords Antarctic phytoplankton · Acclimation · Light availability · Accumulation rates · Standing stock

Introduction

The highly productive Antarctic coastal marine ecosystems are subjected to pronounced seasonality in the light environment. Phytoplankton accumulation begins as the light returns after mid-winter when phytoplankton cells are still subjected to deep mixing and low average light levels (~ 1 µmol quanta m^{-2} s^{-1}; Venables et al. 2013). Although gross growth (μ_{gross}) at this time may be relatively low, a decoupling between phytoplankton μ_{gross} and losses during winter (due to the deepening of the mixed layer that reduces encounter rates between predator and prey) promotes net accumulation in the water column (the Dilution-Recoupling Hypothesis; Behrenfeld 2010). With the seasonal reduction in wind speed promoting a shallowing of the mixed layer after (mid-) winter, a re-coupling of phytoplankton growth and loss processes is offset by concurrent increases in μ_{gross} (mainly due to increasing light availability) until phytoplankton accumulation ceases due to factors limiting growth (e.g. low nutrients, low light or over-predation) (Taylor et al.

T. E. G. Biggs
tristan.biggs@nioz.nl

1 NIOZ Royal Netherlands Institute for Sea Research, Texel and Yerseke, The Netherlands

2 Department of Freshwater and Marine Ecology, Institute for Biodiversity and Ecosystem Dynamics (IBED), University of Amsterdam, Amsterdam, The Netherlands

3 Department of Ocean Ecosystems, University of Groningen, Groningen, The Netherlands

4 Ocean Biogeochemistry & Ecosystems Research Group, National Oceanography Centre, Southampton, UK

5 British Antarctic Survey, Natural Environmental Research Council, Cambridge, UK

6 Institute of Aquaculture, University of Stirling, Stirling, Scotland, UK

2013; Llort et al. 2015; Park et al. 2017; Oliver et al. 2019). Whilst zooplankton grazing is traditionally viewed as the dominant loss factor of phytoplankton cells, more recent studies measuring specific viral lysis rates under natural conditions indicate viral lysis is just as important (Mojica et al. 2016; Biggs et al. 2021). As the response time to seasonal changes in phytoplankton availability could potentially differ between viruses and grazers, another layer of complexity is added when explaining the balance between predator, prey and the observed phytoplankton standing stock.

Rates of accumulation may also be influenced by seasonality in the growth response of phytoplankton (Sloughter et al. 2019). Reduced growth in overwintered populations (after long periods of low PAR) has been related to physiological changes that balance maintenance respiration against photosynthetic efficiency and energy expenditure. If light intensity remains below a certain threshold level, it may be beneficial to decrease maintenance losses, resulting in a reduced ability of phytoplankton growth to respond to increased levels of light. When average light exposure rises above this threshold level, where respiration and gross growth balance (and hence net growth is zero), the net effect can be a shift from a slow to a fast growth response at higher light. Such adaptive variability has been suggested as a response to low light over the winter period, yet, low-light levels may also occur during the productive season (Clarke et al. 2008; Venables and Moore 2010; Venables et al. 2013). Such a response could be beneficial depending on the length of the low-light period and the time taken for phytoplankton to adapt. Variability in ice cover, cloudiness, water column stratification, the frequency, duration and intensity of wind driven mixing, suspended sediments and the degree of self-shading largely determines the light climate during the Southern Ocean productive season (Clarke et al. 2008; Venables and Moore 2010; Ducklow et al. 2012; Venables et al. 2013). A previous study at the Western Antarctic Peninsula (WAP), based in the same area as this study, indicated that light attenuation due to phytoplankton biomass (Biggs et al. 2019) is a major determinant controlling light intensity in the water column (Biggs 2020).

Overall, the response of phytoplankton to light may be at the community level, such as changes in specific dominating species, cell size and/or taxonomic groups, as well as intraspecific variation, such as changes in genotypes or pigment concentrations (Timmermans et al. 2001; Moore et al. 2006; Arrigo et al. 2010; Alderkamp et al. 2012). The growth capability of the community in response to light may have significant impacts on the timing, magnitude and composition of phytoplankton blooms, ultimately influencing top-level consumers (Winder and Sommer 2012). The high biomass phytoplankton blooms that typically develop in polar regions (Thomalla et al. 2011; Llort et al. 2015) limit the penetration of light into the water column (Vernet et al. 2008; Park et al. 2017) and can span considerable time periods during the growth season (Arrigo et al. 2015). As such, acclimation to low-light levels is likely of critical importance in relation to potential growth. The response of natural communities to light is argued to have important implications for marine productivity models, especially for predictions in rapidly changing environments (Sloughter et al. 2019). Yet, the role of light in controlling peak biomass and seasonal dynamics in Antarctic waters is less clear (Arrigo et al. 2015).

Whilst many Southern Ocean studies have used pigment analysis to describe the phytoplankton community (e.g. Wright et al. 2010; Kozlowski et al. 2011; Mendes et al. 2012), very few have combined this with flow cytometry to discriminate different populations in more detail (García-Muñoz et al. 2013). Although phytoplankton pigment analysis via high-performance liquid chromatography (HPLC), followed by chemical taxonomy (CHEMTAX; Mackey et al. 1996) provides a taxonomic classification of the phytoplankton community (Wright and Van den Enden 2000; Wright et al. 2010), acclimation due to changing cellular pigment concentrations (Dubinsky and Stambler 2009) could potentially skew estimates of biomass concentrations and taxonomic contributions based on pigments. Furthermore, a relatively few large cells can dominate total Chl-*a*, obscuring the changes within smaller-sized populations. Flow cytometry is based on single-cell analysis (of pigment autofluorescence and scatter signals) and offers a greater level of differentiation of the phytoplankton community. In addition, combining these techniques with size fractionation can provide a rapid and more detailed assessment of multiple phytoplankton populations within a single taxonomic group (Biggs et al. 2019).

Understanding the ecological and physiological mechanisms driving Antarctic phytoplankton community structure is vital to assess the response of marine systems to global climate change. Shifts in size class distribution have the potential to drastically alter the Southern Ocean food web (Atkinson et al. 2004). Global warming is expected to indirectly affect light availability as a result of prolonged and intensified vertical stratification or increased mixing, depending on regional differences (Meredith et al. 2022). Such changes could cause shifts in Antarctic phytoplankton community composition (Garibotti et al. 2005; Mendes et al. 2017; Biggs et al. 2019) which will alter trophic transfer efficiency and elemental cycling (Petrou et al. 2016; Rembauville et al. 2016). In addition, reductions in sea ice duration and extent will also lengthen the productive season, primarily due to increased light availability in the water column in spring and autumn (Montes-Hugo et al. 2009; Arrigo and van Dijken 2015).

The aim of this study was to examine in more detail, by combining taxonomic classification, flow cytometric single-cell analysis and size fractionation, to what extent

light influences the composition, standing stock and net accumulation rates of Antarctic phytoplankton. Six incubation experiments were performed on seawater collected from a coastal site at the WAP during the main productive season (December to March), using 3 light intensities (low, medium, high; ranging from 4 to 200 µmol quanta m^{-2} s^{-1}). We hypothesize that specific phytoplankton populations are able to adjust their growth potential under low-light levels and as such, extend periods of accumulation. Although we expect, from the literature, diatoms to be competitive under low light (Petrou et al. 2016; Rozema et al. 2017b; Strzepek et al. 2019), we also hypothesize that some diatoms may be better adapted to low-light conditions (e.g. diatom Phyto IX, 11.5-µm cell diameter; as suggested by Biggs et al. 2019), whilst others are more competitive under high and medium light (diatom Phyto VI, 4.5 µm diameter; Biggs et al. 2019).

Methods

Physiochemical measurements

Data for this study were obtained from the Rothera time series site (RaTS, latitude 67.572° S; longitude 68.231° W; Clarke et al. 2008) located in Ryder Bay on the Western Antarctic Peninsula (WAP, Fig. 1). Environmental conditions were recorded over two austral productive periods, season 1 (S1) from Dec 2012 to April 2013 and season 2 (S2) between Nov 2013 and April 2014 (Biggs et al. 2019). Water column profiles were obtained using a SeaBird 19 + conductivity temperature depth instrument (CTD) supplemented with a flat LiCor sensor to measure photosynthetically available radiation (PAR) and an in-line fluorescence sensor (WetLabs). CTD deployment was from a rigid inflatable boat, using a handcranked winch, with casts conducted to near-seabed (500 m). Full details are available in Meredith et al. (2004) and Clarke et al. (2008). In situ density, temperature, salinity (as expressed on the Practical Salinity Scale used throughout this paper) and PAR at the sampling depth were obtained from the CTD. In addition, detailed time series data (and methologies) of other environmental conditions, such as sea ice coverage, mixed layer depth (MLD; defined here as the depth at which the density is greater than the surface density by 0.05 kg m^{-3}), stratification level (potential energy required to homogenize the water column from the surface to 40 m depth) and dissolved inorganic phosphate, nitrate and silicate concentrations are published in Biggs et al. (2019). Daily air-PAR (24 h average of light intensity readings) were recorded at a weather station on top of a hill at Rothera Station (British Antarctic Survey).

Light experiments

Seawater for the incubation experiments was collected at the RaTS long-term monitoring site (at 15 m depth) by a 12-L Niskin bottle deployed from a small boat. As MLD was very shallow during summer (< 4 m at the start of INC 3–5 and 8–12 m for INC 1, 2 and 6), seawater samples for all experiments were collected from below the mixed layer. Taking care to prevent light exposure, the 24-L polycarbonate Nalgene carboys (used for the incubations) were filled to the brim. Seawater was transported to a temperature-controlled lab maintained at ~ 0.5 °C, immediately sub-sampled (20 L final volume) and then transferred (whilst kept dark) to an indoor flow-through (seawater) incubator to replicate in situ temperature dynamics. Three PAR intensities were used for each experiment of 150–200 (high light, HL), 30–50 (medium light, ML) and 4–7 µmol quanta m^{-2} s^{-1} (low light, LL). Photosynthesis irradiance measurements on seawater collected at the same sample site during S2 are published in Rozema et al. (2017a). These data indicate that during this season (Nov–Mar) E_K ranged from 34 to 68 µmol

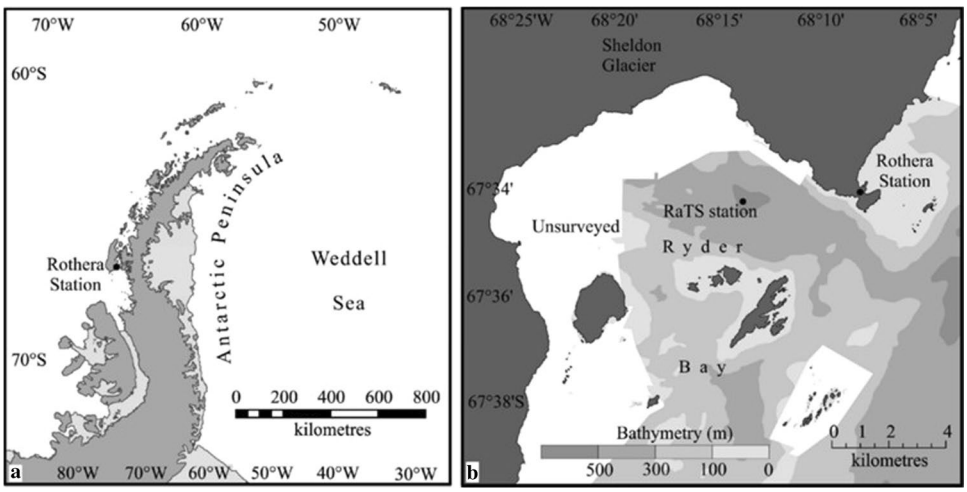

Fig. 1 Map of the location of **a** Rothera Station on the Western Antarctic Peninsula and **b** the Rothera Time Series sample site (RaTS station) in relation to Rothera station

quanta m^{-2} s^{-1}, similar to medium light levels used during incubations. Unfortunately, photosynthesis irradiance measurements were not available for S1. For each light treatment triplicate bottles were incubated, hence nine bottles in total. Light was supplied by 18 W/965 OSRAM daylight spectrum fluorescent tubes (München, Germany) and the light intensity was adjusted using neutral density screens. Incubation bottles were turned three times a day to simulate water column mixing.

To best mimic natural phytoplankton dynamics, we used untreated natural seawater for the incubation experiments. We aimed to study net phytoplankton community dynamics and constraining top-down controls (e.g. grazers and viruses) would skew the results. Firstly, not all grazers (different size classes) can be removed without also affecting the phytoplankton community. Secondly, removing only the larger grazers (e.g. > 200 µm) affects the grazing impact of the microzooplankton as they are also potential prey for larger zooplankton. Furthermore, removing viruses (by filtration or dilution) affects not only the phytoplankton dynamics but also the numerically dominant bacterial hosts. Unlike phytoplankton, we anticipate zooplankton not to be directly affected by light intensity; therefore, we expect that grazers and viruses are not driving the response of phytoplankton to light availability. Although changes in the grazer and virus community may occur during the incubations, these alterations would likely be in response to changes in phytoplankton availability and community composition. This is one of the reasons we limited the incubations to 9–10 days.

Six incubation experiments (INC) were performed in total: INC 1 and 2 lasted 10 days and were conducted during the second half of S1 on 6 Feb and 11 Mar (2013). INC 3–6 were performed over 9 days and conducted over S2 on 4 and 28 Dec 2013 and 29 Jan and 25 Feb 2014 (Table 1). At the beginning (T_0) and end (T_{END}) of each incubation, 6-mL subsamples were collected for nutrients (phosphate, nitrate and silicate) and 1-L subsamples for phytoplankton pigment analysis (apart from T_0 for INC 1 and 2 where only 2 × 1-L subsamples were taken for pigment analysis, from the first and last bottle of seawater collected). On day 0 (T_0), day 3 (T_3), day 7 (T_7) and day T_{END}, 55-mL subsamples were collected for phytoplankton enumeration and photosynthetic efficiency analysis.

Table 1 List of Incubation experiments (INC) detailing season (Season 1 or 2; S1 or S2, respectively) and start date

Incubation experiment	Season	Date
INC 1	S1	6 Feb 2013
INC 2	S1	11 Mar 2013
INC 3	S2	4 Dec 2013
INC 4	S2	28 Dec 2013
INC 5	S2	29 Jan 2014
INC 6	S2	25 Feb 2014

Phytoplankton variables

Photosynthetic efficiency (F_v/F_m) was determined using pulse amplitude-modulated (PAM) fluorometry (Water-PAM). Samples were dark acclimated for 15 min on ice after which the minimum (F_0) and maximum (F_m) chlorophyll fluorescence were measured. The variable fluorescence (F_v) is calculated as $F_m - F_0$ (Maxwell and Johnson 2000). For comparison of F_v/F_m between and within experiments, we attempted to maintain a constant Gain setting of 7. However, low Chl-*a* concentrations at the beginning of S2 required a Gain setting of 9 to be used throughout INC 3.

Samples for Chl-*a* concentration and phytoplankton taxonomic composition (based on pigment ratios) were obtained by filtering 1 L through GF/F glass fibre filters (47 mm, Whatman, the Netherlands). Filters were wrapped in aluminium foil, snap-frozen in liquid nitrogen and stored at − 80 °C until analysis. Phytoplankton pigments were analysed by high-performance liquid chromatography (HPLC) according to Brussaard et al. (2016) and pigment quantification was performed using reference standards (DHI, Hørsholm, Denmark). Peaks identified were manually checked for quality assessment. Phytoplankton class abundances were calculated using pigment data from HPLC by CHEMTAX v1.95 (Mackey et al. 1996). This programme uses a factor analysis and steepest decent algorithm to find the best fit based on a pigment ratio matrix. Six taxonomic classes were chosen to classify the WAP phytoplankton, in line with those used previously for RaTS site data (Biggs et al. 2019) and confirmed by microscopy observations (unpublished data): Prasinophyceae, Chlorophyceae, Dinophyceae, Cryptophyceae, Prymnesiophyceae and Bacillariophyceae (diatoms). CHEMTAX was run 60 times using all pigment concentration data with randomized (± 35%) pigment ratios to minimize the root mean square error (RMSE) using settings recommended in Kozlowski et al. (2011). The run with the lowest RMSE was deemed final with initial and final ratios shown in Online Resource 1. Chl-*a* concentrations were converted to cellular carbon (Chl-C) using taxon-specific conversion factors according to Garibotti et al. (2003), with the exception of Dinophyceae for which we used an average of ratios by Llewellyn et al. (2005) and Agirbas et al. (2015). Specific accumulation (net growth) rates (day^{-1}) were determined for the different phytoplankton taxonomic groups, as well as for total Chl-*a* and Chl-C over the entire incubation period, i.e. T_0 to T_{END}. Significant differences between light treatments and experiments were tested using a one-way analysis of variance (ANOVA or ANOVA on Ranks when unequal variance was detected; SigmaPlot v14, from Systat Software, Inc., San Jose California, USA), a two-tailed Student's *t* test

or Wilcoxon Signed Rank Test for non-normal data (SigmaPlot v14).

For flow cytometric phytoplankton enumeration, 3.5-mL subsamples were fixed with 100-µL formaldehyde–hexamine (18% v/v:10% w/v) at 4 °C, after which they were snap-frozen in liquid nitrogen and stored at − 80 °C until analysis. Samples were analysed according to Marie et al. (1999) using a Becton Dickinson FACSCalibur flow cytometer (BD Biosciences) equipped with an air-cooled Argon laser with an excitation wavelength of 488 nm (15 mW). The trigger was set on red fluorescence channel and phytoplankton populations were distinguished using bivariate scatter plots of red chlorophyll-*a* (Chl-*a*) autofluorescence versus side scatter. Cryptophytes were discriminated based on their orange phycoerythrin autofluorescence. Furthermore, seawater samples were size fractionated by gentle (largely by gravity) serial filtration of a small volume of sample. Ten phytoplankton groups were discriminated, coded Phyto I to X, with average cell diameters of 0.9, 1.8, 3.1, 4.0, 4.5, 4.5, 7.4, 8.1, 11.5 and 20.4 µm, respectively (Biggs et al. 2019). Based on the flow cytometry data in combination with published < 20-µm Chl-*a* concentrations and chemical taxonomy results by Biggs et al. (2019), the larger algal groups Phyto V–X were classified as diatoms, Phyto IV as cryptophytes (Cryptophyceae; based on orange autofluorescence and microscopy) and Phyto III as *Phaeocystis* spp. (based on microscopy and resembling temporal dynamics with Prymnesiophyceae). Light microscopy of Lugol's fixed seawater samples in S1 (unpublished data) shows that two days after the start of INC 2 (corresponding to peak abundance of Phyto IX), nano-sized centric diatoms (9–17 µm) dominated the phytoplankton community. Although we did not specifically quantify or identify the diatoms via microscopy, van Leeuwe et al. (2020) observed at the same location in January/February 2013 relatively high numbers of *Thalassiosira* spp. (5–20-µm cell length) and *Chaetoceros* spp. (10–15-µm cell length). The authors also show relatively high numbers of *Chaetoceros* spp. (10–15 µm) and various *Fragilariopsis* species between November 2013 and February 2014.

Cellular carbon contents for the phytoplankton populations identified by flow cytometry (FCM-C) were derived using their average cell diameter (assuming cells to be spherical) and conversion factors of 196.5 and 237 fg C μm^{-3} for nano- and pico-sized phytoplankton populations, respectively (Garrison et al. 2000; Worden et al. 2004).

Specific accumulation (net growth) rates (day^{-1}) were calculated from the abundance dynamics for the different phytoplankton groups as well as for total phytoplankton (the latter both based on cell count and cellular carbon) over the entire incubation period, i.e. T_0 to T_{END} (10 days for INC 1 and 2 and 9 days for INC 3–6). Additionally, we calculated the accumulation (net growth) rates specifically for the start ($T_{0–3}$ days), mid ($T_{3–7}$ days) and end ($T_{0–END}$) of the incubations.

Results

Incubation starting conditions

The environmental conditions at the time of sampling for the incubation experiments are listed in Table 2. In short, the seawater temperature at the start of the experiments was above 0 °C for INC 1, 2 and 5 (i.e. 1.2, 0.7 and 0.5 °C, respectively) and below 0 °C for INC 3, 4 and 6 (− 0.8, − 1.0 and − 0.5 °C). Note that during the 21 days prior to the start of the incubations, the average temperature was ≥ 1 °C for INC 1 and 2 and ≤ 0 °C for INC 3–6. INC 5 showed the largest difference in temperature (0.7 °C), ranging from below to above 0 °C. Although there was more ice cover in the latter half of productive season S1 (INC 1 and 2) when compared with the same period in S2 (INC 5 and 6), ice melt was most visible in the relatively low salinity of the seawater used to setup INC 5. Dissolved inorganic phosphate and nitrate concentrations were lowest at the start of INC 2 and 5 (< 0.3 and < 7.9 µM, respectively), whilst silicate concentrations were > 25 µM for all experiments. Mean daily air-PAR is largely determined by day length and was consequently lowest at the end of the productive season, both for S1 and S2 (6 and 16 µmol quanta m^{-2} s^{-1} for INC 2 and 6, respectively; Table 2). Similar to air-PAR, the PAR intensities at the 15-m sampling depth were low for INC 2 and highest at the beginning of INC 3 (0.3 and 310 µmol quanta m^{-2} s^{-1}, respectively). Whilst PAR levels were low in the water column at the time of sampling for INC 4 and 5, they had been considerably higher in the preceding period (i.e. average PAR 26 and 23 µmol quanta m^{-2} s^{-1}; Table 1).

The phytoplankton community in the natural seawater used for INC 1 (0.7 ± 0.1 µg Chl-*a* L^{-1}, $n = 2$, Fig. 2a) seeded a high biomass bloom under natural conditions (Biggs et al. 2019) composed of equal proportions of diatoms, cryptophytes and prymnesiophytes (32 ± 2, 33 ± 5 and 31 ± 5%, $n = 2$; Online Resource 2 and 3). Specifically, diatom Phyto VI and Phyto III (i.e. *Phaeocystis* spp.) dominated total phytoplankton abundance (56 ± 5 and 19 ± 4%, $n = 8$, respectively; Fig. 2b and Online Resource 4 and 5). Cellular carbon was largely composed of Phyto VI (44 ± 5%, $n = 8$), but also the larger-sized Phyto IX (26 ± 2% of total, $n = 8$; Online Resource 6). INC 2 had the highest Chl-*a* starting concentration (16.9 ± 1 ug L^{-1}, $n = 2$; Fig. 2a) and phytoplankton abundances (5.1 ± 1.1 × 10^3 cells mL^{-1}, $n = 9$; Fig. 2b), representing a diatom-dominated bloom climax (Chl-*a* 99 ± 0.1%, Chl-C 100 ± 0%, $n = 2$; Online Resource 2, 3 and 7). Phyto IX comprised 66 ± 5% of total counts ($n = 9$;

Table 2 Environmental conditions at the sample site (on the day of sampling) for incubations 1–6 (INC 1–6) at T_0 (6 Feb and 11 Mar 2013, 4 and 28 Dec 2013 and 29 Jan and 25 Feb 2014, respectively) and as average of 3 weeks prior to the start of the incubations (21 day mean): Temperature (Temp.), ice cover, salinity, photosynthetically active radiation (PAR) in air, PAR at sampling depth, level of stratification over the top 40 m of the water column (Strat.), dissolved inorganic nitrate (NO_3) and phosphate (PO_4) concentrations, nitrate-to-phosphate ratio (NO_3:PO_4), and silicate (Si) concentrations

	Temp (°C)	Ice cover (%)	Salinity	Air PAR day^{-1} (µmol quanta m^{-2} s^{-1})	PAR (µmol quanta m^{-2} s^{-1})	Strat (J m^{-2})	NO_3 (µM)	PO_4 (µM)	NO_3:PO_4	Si (µM)
At T_0										
INC 1	1.2	20	33.2	30	40	433	14	1.1	13	58
INC 2	0.7	40	33.2	6	0.3	231	7.9	0.3	28	58
INC 3	− 0.8	40	33.7	69	310	365	27	1.9	14	79
INC 4	− 1.0	30	33.6	44	3.0	911	25	1.8	14	74
INC 5	0.5	10	32.8	49	7.0	997	3.9	0.2	18	25
INC 6	− 0.5	10	33.3	16	32	684	18	1.4	13	55
21-day mean										
INC 1	1.3	24	33.3	33	24	573	13	0.9	14	57
INC 2	1.0	31	33.2	21	2.0	424	11	0.4	27	57
INC 3	− 1.2	25	33.8	43	139	193	28	1.8	16	81
INC 4	− 0.5	63	33.6	47	26	887	22	1.5	15	68
INC 5	− 0.2	23	33.0	42	23	955	9.2	0.5	18	34
INC 6	0.0	16	33.0	26	39	617	12	0.9	13	40

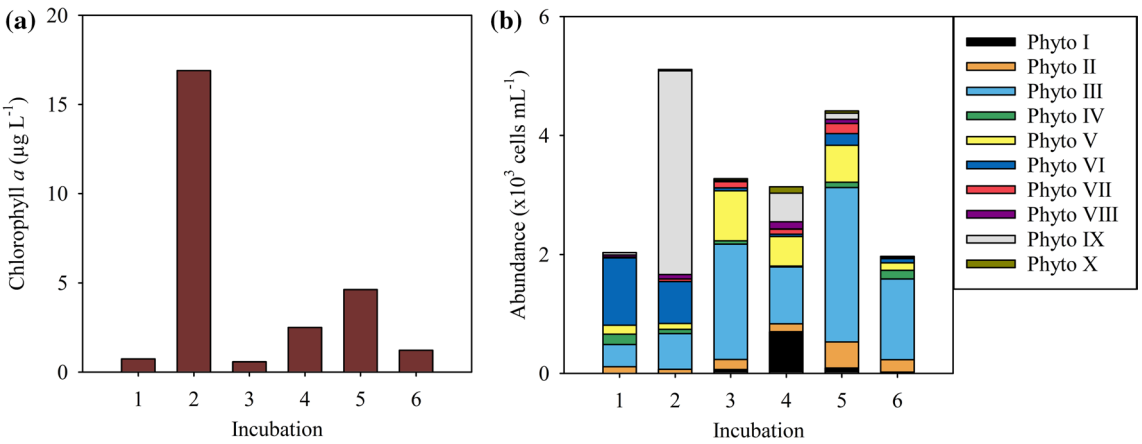

Fig. 2 The phytoplankton community at the start of the six incubation experiments in terms of **a** total chlorophyll-*a* and **b** community composition as determined by flow cytometric identification of the ten distinct groups designated Phyto I–X (respectively)

Online Resource 4) and 94 ± 5% (n = 9) of cellular carbon (533 ± 143 µg L^{-1}, n = 9; Online Resource 6).

During S2, INC 3 was setup with seawater containing the start community of the initial phytoplankton bloom (0.6 ± 0.1 µg Chl-*a* L^{-1}, n = 9), consisting mostly of diatoms (89 ± 1% n = 9) and to a lesser extent prymnesiophytes (10%, Online Resource 2). *Phaeocystis* spp. Phyto III represented the majority (59 ± 1% n = 9; Online Resource 4) of the initial total phytoplankton cell abundance (3.3 ± 0.1 × 10^3 cells mL^{-1}, n = 9; Online Resource 8), with diatom Phyto V being the second most abundant (26 ± 2% n = 9; Fig. 2b and Online Resource 4). Cellular carbon was dominated by the larger-sized Phyto X (51 ± 6%, n = 9) and to a lesser extent by Phyto III (15 ± 2%, n = 9) and Phyto V (17 ± 3%, n = 9; Online resource 9). At the time of INC 4, the diatom-dominated (97 ± 1%, n = 9; Online Resource 3) Chl-*a* concentrations were relatively high (2.5 ± 0.5 µg L^{-1} n = 9, Fig. 2a). In particular, Phyto IX and Phyto X (484 ± 140 and 106 ± 43 cells mL^{-1}, n = 9; Online resource 4) made up 41 ± 7 and 48 ± 7% (n = 9) of cellular carbon, respectively

(Online Resource 9). Chl-*a* concentrations were still high at the start of INC 5 (4.6 ± 0.3 µg L^{-1}, $n = 9$; Fig. 2a), again primarily due to diatoms ($87 \pm 3\%$, $n = 9$) but with increased contributions of Prymnesiophyceae ($11 \pm 2\%$, $n = 9$; Online Resource 2). The share of *Phaeocystis* spp. Phyto III was similar to the start community for INC 3 but its abundance was a factor of 1.3 higher (2.6×10^3 cells mL^{-1}, $n = 9$; Fig. 2b). Diatoms Phyto IX and Phyto X remained the primary contributor to the phytoplankton cellular carbon pool (21 ± 3 and $41 \pm 8\%$, respectively, $n = 9$; Online Resource 9). Seawater for INC 6 was collected after the decline of the initial S2 phytoplankton bloom (Chl-*a* reduced to 1.2 ± 0.1 µg L^{-1}, $n = 9$; Fig. 2a). The contributions of cryptophytes and prymnesiophytes had increased (18 ± 3 and $22 \pm 5\%$, respectively, $n = 9$) but diatoms still dominated the phytoplankton community ($56 \pm 6\%$ of total Chl-*a*, $n = 9$; Online Resource 2). Total phytoplankton abundance was $2 \pm 0.1 \times 10^3$ cells mL^{-1} ($n = 9$; Fig. 2b) and largely represented by *Phaeocystis* spp. Phyto III ($69 \pm 2\%$, $n = 9$) and picoeukaryote Phyto II ($11 \pm 1\%$, $n = 9$; Online Resource 4). Despite their low abundance (< 11 cells mL^{-1}, Fig. 2b), the larger-sized Phyto IX and X comprised $41 \pm 10\%$ ($n = 9$) of total cellular carbon (Online Resource 9).

Photosynthetic efficiency and chlorophyll-a

The photosynthetic efficiency (F_v/F_m) at the start of all experiments indicated that phytoplanktons were not photosynthetically stressed, i.e. values between 0.54 and 0.71 (Fig. 3). For the LL and ML treatments F_v/F_m stayed high during the 9- or 10-day incubations. The F_v/F_m ratios initially dropped slightly in all the HL experiments, with some recovery in INC 3 and 5 (Day 3 to 7). Unlike for the other experiments, ambient light levels preceding the setup of INC 2 were very low (Table 1), which may explain the steady drop in F_v/F_m under HL over the ten days of INC 2 (minimum 0.26; Fig. 3).

At the end of all incubation experiments, diatoms dominated total Chl-*a* concentrations, independent of the light levels (Online Resource 3). Also for INC 1, starting with a relatively low share of diatoms ($32 \pm 2\%$, $n = 2$), diatoms contributed most to total Chl-a towards the end of the experiment (87 ± 8, 81 ± 4, and $60 \pm 5\%$, $n = 3$, for HL, ML and LL, respectively). Chl-*a* concentrations (similar to Chl-C) at the end of INC 1 and 6 were significantly lower under LL compared to ML and HL (Fig. 4a, b; ANOVA: $F_{2,5}$ (INC 1) $F_{2,6}$ (INC 6) = 352, 40, respectively, $p < 0.001$). Prasinophyte Chl-*a* concentrations were greatest at the end of INC 1 and 6 under HL and ML (compared to LL; Online Resource 3), the only experiments where prasinophyte Chl-*a* was significantly different between light treatments (ANOVA: $F_{2,5}$ and $F_{2,6} = 58.9$ and 42.7, respectively, $p < 0.001$; Online Resource 3). In contrast to INC 1 and 6,

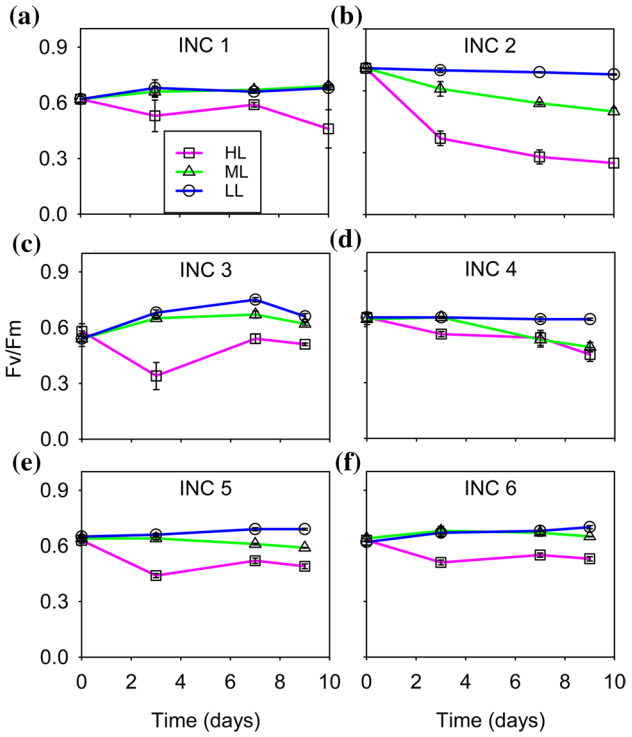

Fig. 3 The influence of light on the photosynthetic efficiency (F_v/F_m) of the phytoplankton community under the light regimes 150–200 (high light, HL), 30–50 (medium light, ML) and 4–7 µmol quanta m^{-2} s^{-1} (low light, LL) during incubation experiments (INC) 1–6 (**a** to **f**, respectively). Error bars represent ± 1 standard deviation

Chl-*a* concentrations (and also Chl-C) at the end of INC 2, 3, 4 and 5 (Online Resource 3) were significantly higher under LL compared to HL and ML (Fig. 4a, b; ANOVA: $F_{2,6}$ (INC 2, 3 and 5) $F_{2,5}$ (INC 4) = 20.2, 7.5, 37.8 and 11.9 $p = 0.002$, 0.023, < 0.001 and 0.012, respectively). Chl-*a* and Chl-C accumulation rates were also lowest under LL in INC 1 and 6 and highest under LL in INC 2–5 (Fig. 5a, b).

Flow cytometry

At the end of the incubations, total phytoplankton abundances as determined by flow cytometry (FCM-ab) were significantly lower under LL (compared to HL or ML) in all experiments apart from INC 2 (ANOVA on ranks: $H_2 = 6.3$, $p = 0.011$, 0.011, (INC 1, 4); ANOVA: $F_{2,5} = 23$, $p = 0.003$ (INC 3); $F_{2,6} = 145$, 239, $p < 0.001$, < 0.001 (INC 5, 6, respectively); Fig. 4 c and Online Resource 5 and 8). Similarly, flow cytometry-based abundance (and carbon) accumulation rates were significantly lower under LL (compared to HL or ML) in all experiments apart from INC 2 (ANOVA: $F_{2,5}$ (INC 1 and 4) $F_{2,6}$ (INC 3, 5 and 6) = 35, 25, 9.9, 346, 108, $p = 0.001$, 0.002, 0.013, < 0.001, < 0.001, respectively; Fig. 5c, d and Tables 3 and 4). For INC 1, 3, 4, 5 and 6 under LL, phytoplankton numbers were merely

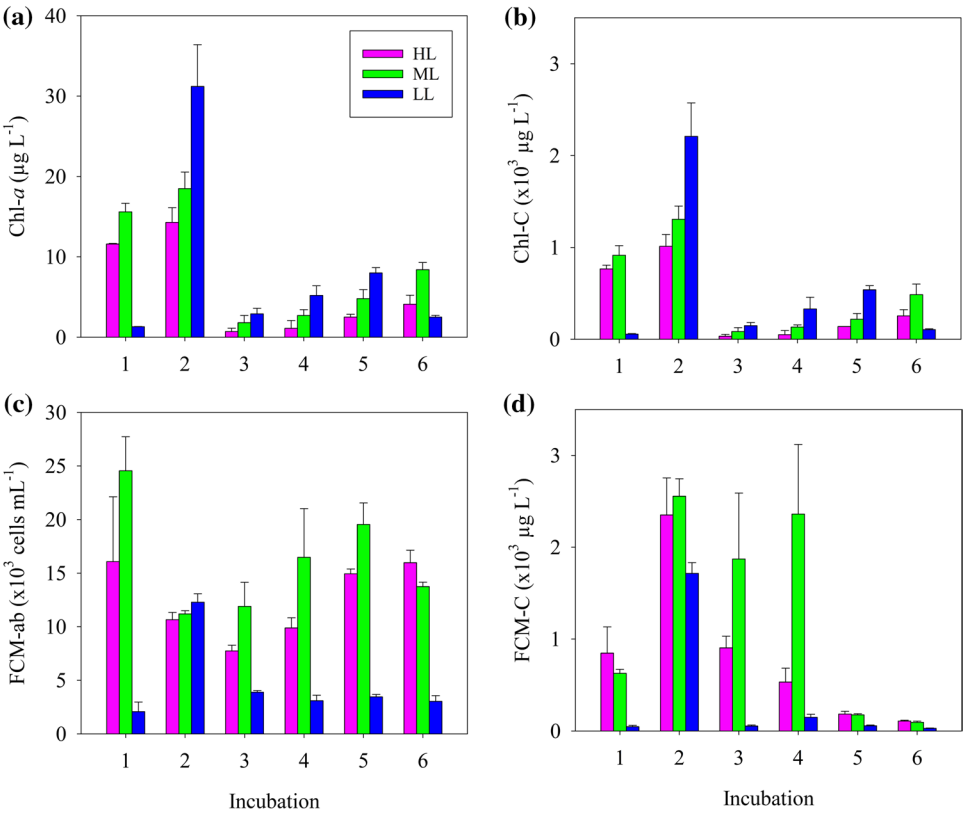

Fig. 4 Phytoplankton **a** chlorophyll-*a* (Chl-*a*) concentrations, **b** chlorophyll-based carbon (Chl-C), **c** flow cytometry abundances (FCM-ab) and **d** abundance-based carbon (FCM-C) at the termination of incubation experiments (INC) 1 to 6. Error bars are calculated from triplicates and represent + 1 standard deviation

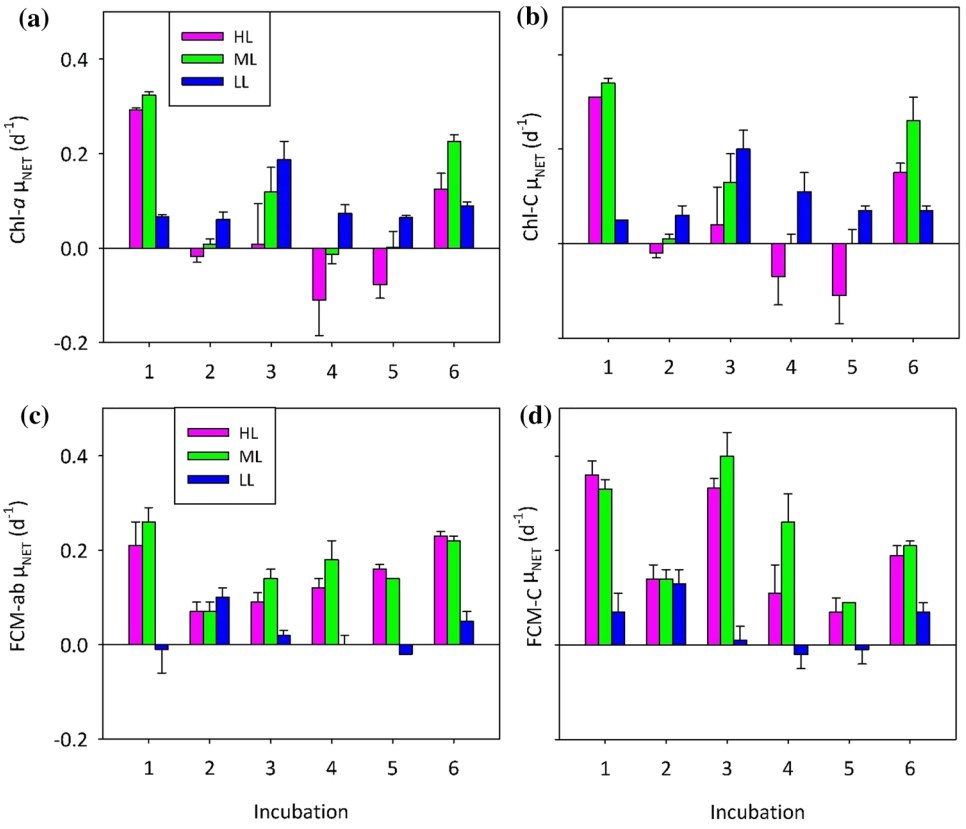

Fig. 5 Phytoplankton net growth rates (μ_{NET}) calculated over the full duration of the incubations according to **a** chlorophyll-*a* (Chl-*a*), **b** estimated chlorophyll carbon (Chl-C), **c** total phytoplankton abundance (FCM-ab) and **d** estimated phytoplankton carbon (FCM-C). Error bars are calculated from triplicates and represent + 1 standard deviation

Table 3 Accumulation rates (day^{-1}) of Phyto I to X as well as total phytoplankton abundance (FCM-ab) and carbon (FCM-C) during Season 1 in INC 1 and 2

INC	Light level	Time period	Phyto I	Phyto II	Phyto III	Phyto IV	Phyto V	Phyto VI	Phyto VII	Phyto VIII	Phyto IX	Phyto X	FCM -ab	FCM -C
1	HL	$T_{0–3}$	0.25	0.29	− 0.18	− 0.07	0.13	− 0.27	− 0.05	0.00	0.39	0.00	− 0.06	0.11
1	HL	$T_{3–7}$	0.01	0.01	0.02	− 0.06	0.23	0.00	0.39	0.13	0.36	− 0.14	0.10	0.33
1	HL	$T_{7–10}$	− 0.60	0.27	0.40	0.06	0.32	0.44	0.05	0.27	0.59	0.23	0.40	0.49
1	HL	$T_{0–END}$	NA	0.22	0.18	0.08	0.27	0.14	0.20	0.12	0.48	− 0.09	0.21	0.36
1	ML	$T_{0–3}$	− 0.44	0.43	0.36	0.04	0.28	0.30	0.31	0.28	0.36	N/A	0.31	0.33
1	ML	$T_{3–7}$	0.10	0.16	0.23	− 0.12	0.23	0.19	0.00	0.24	0.45	0.24	0.20	0.31
1	ML	$T_{7–10}$	0.46	0.17	0.21	0.09	0.03	0.33	0.10	0.10	0.46	0.11	0.29	0.39
1	ML	$T_{0–END}$	0.13	0.23	0.25	− 0.03	0.14	0.27	0.12	0.22	0.42	N/A	0.26	0.33
1	LL	$T_{0–3}$	− 0.21	0.08	− 0.01	− 0.03	− 0.02	− 0.03	− 0.23	0.06	0.24	N/A	− 0.01	0.08
1	LL	$T_{3–7}$	N/A	− 0.16	− 0.14	− 0.17	− 0.01	− 0.10	0.18	0.13	0.12	− 0.14	− 0.08	0.03
1	LL	$T_{7–10}$	N/A	− 0.05	− 0.08	0.07	0.20	0.09	0.52	0.10	0.09	0.18	0.09	0.11
1	LL	$T_{0–END}$	− 0.05	− 0.06	− 0.08	− 0.05	0.05	− 0.02	0.16	0.10	0.14	N/A	− 0.01	0.07
2	HL	$T_{0–3}$	N/A	− 0.27	− 0.08	− 0.11	− 0.03	0.28	0.05	0.09	0.24	1.02	0.22	0.36
2	HL	$T_{3–7}$	N/A	0.34	0.00	− 0.06	− 0.01	− 0.05	0.00	− 0.03	0.03	0.14	0.02	0.07
2	HL	$T_{7–10}$	0.12	− 0.12	− 0.08	0.01	0.02	− 0.20	− 0.01	− 0.02	− 0.01	0.03	− 0.02	0.02
2	HL	$T_{0–END}$	N/A	0.02	− 0.05	− 0.05	− 0.01	0.01	0.01	0.01	0.08	0.37	0.07	0.14
2	ML	$T_{0–3}$	− 0.07	− 0.18	0.11	− 0.07	0.07	0.21	0.07	0.08	0.24	1.14	0.23	0.35
2	ML	$T_{3–7}$	0.00	0.17	− 0.12	− 0.12	− 0.10	0.00	0.06	0.12	0.01	− 0.07	0.00	− 0.01
2	ML	$T_{7–10}$	N/A	− 0.29	− 0.06	− 0.69	− 0.02	− 0.19	0.02	− 0.02	− 0.01	0.43	0.01	0.14
2	ML	$T_{0–END}$	N/A	− 0.07	− 0.03	− 0.28	− 0.02	0.01	0.05	0.07	0.07	0.44	0.07	0.14
2	LL	$T_{0–3}$	− 0.27	0.09	0.20	− 0.07	0.24	0.05	0.33	0.17	0.32	− 0.03	0.26	0.31
2	LL	$T_{3–7}$	N/A	− 0.07	− 0.02	− 0.08	− 0.02	− 0.01	0.05	0.05	0.11	0.19	0.08	0.11
2	LL	$T_{7–10}$	N/A	− 0.24	− 0.19	− 0.10	− 0.13	− 0.12	− 0.10	0.07	− 0.01	0.18	− 0.03	− 0.01
2	LL	$T_{0–END}$	N/A	− 0.07	− 0.01	− 0.08	0.03	− 0.02	0.09	0.09	0.14	0.12	0.10	0.13

N/A represents missing data due to one or more zero counts in each set of triplicates

Table 4 Accumulation rates (day^{-1}) of Phyto I to X as well as total phytoplankton abundance (FCM-ab) and carbon (FCM-C) during Season 2 in INC 3–6

INC	Light level	Time period	Phyto I	Phyto II	Phyto III	Phyto IV	Phyto V	Phyto VI	Phyto VII	Phyto VIII	Phyto IX	Phyto X	FCM -ab	FCM -C
3	HL	$T_{0–3}$	− 0.14	− 0.17	0.10	− 0.08	0.34	− 0.33	− 0.16	0.14	− 0.09	0.35	0.16	0.27
3	HL	$T_{3–7}$	0.42	0.05	0.17	0.19	0.18	0.50	− 0.02	1.04	0.74	0.82	0.24	0.73
3	HL	$T_{7–9}$	− 0.10	0.45	− 0.24	− 0.31	− 0.28	− 0.08	0.15	− 0.44	0.17	− 0.42	− 0.24	− 0.38
3	HL	$T_{0–END}$	0.16	0.07	0.05	− 0.04	0.10	0.11	− 0.05	0.44	0.31	0.40	0.09	0.33
3	ML	$T_{0–3}$	− 0.24	− 0.17	0.05	0.00	0.34	− 0.33	− 0.08	0.39	0.21	0.31	0.14	0.26
3	ML	$T_{3–7}$	0.14	0.06	0.18	0.05	0.17	0.48	− 0.24	0.74	0.45	0.62	0.20	0.53
3	ML	$T_{7–9}$	0.23	0.41	− 0.10	− 0.01	− 0.04	0.02	0.17	0.25	0.43	0.37	0.02	0.35
3	ML	$T_{0–END}$	0.03	0.06	0.08	0.02	0.18	0.11	− 0.10	0.51	0.37	0.46	0.14	0.40
3	LL	$T_{0–3}$	− 0.39	0.06	− 0.01	− 0.06	0.12	0.07	0.00	− 0.37	0.09	0.07	0.03	0.06
3	LL	$T_{3–7}$	− 0.22	− 0.07	0.03	0.01	0.11	− 0.22	− 0.13	0.25	− 0.13	− 0.12	0.05	− 0.03
3	LL	$T_{7–9}$	0.07	− 0.15	− 0.11	− 0.03	0.00	0.37	0.32	0.49	0.02	0.06	− 0.04	0.03
3	LL	$T_{0–END}$	− 0.21	− 0.04	− 0.01	− 0.02	0.09	0.01	0.01	0.13	− 0.02	− 0.02	0.02	0.01
4	HL	$T_{0–3}$	0.08	0.19	0.06	0.03	− 0.10	0.29	0.42	0.46	− 0.08	− 0.03	0.08	0.01
4	HL	$T_{3–7}$	0.03	0.14	0.19	− 0.03	0.54	0.21	0.49	0.23	0.51	0.54	0.31	0.49
4	HL	$T_{7–9}$	− 0.42	0.15	− 0.03	0.15	− 0.20	0.26	− 0.34	− 0.10	− 0.34	− 0.67	− 0.18	− 0.44
4	HL	$T_{0–END}$	− 0.09	0.19	0.09	0.01	0.16	0.30	0.33	0.27	0.12	0.05	0.12	0.11
4	ML	$T_{0–3}$	0.13	0.23	0.13	− 0.05	0.04	0.00	− 0.11	0.27	− 0.10	0.19	0.10	0.11
4	ML	$T_{3–7}$	− 0.21	0.18	0.19	− 0.08	0.27	0.43	0.53	0.46	0.51	0.54	0.29	0.51
4	ML	$T_{7–9}$	− 0.50	− 0.23	− 0.31	0.06	0.31	0.27	− 0.73	0.31	0.19	− 0.11	0.05	0.00
4	ML	$T_{0–END}$	− 0.16	0.10	0.06	− 0.05	0.20	0.25	0.03	0.37	0.24	0.28	0.18	0.26
4	LL	$T_{0–3}$	0.02	0.04	0.07	− 0.07	− 0.02	0.11	0.00	− 0.10	0.15	0.06	0.06	0.10
4	LL	$T_{3–7}$	− 0.22	− 0.10	0.00	− 0.14	0.03	− 0.05	0.00	0.26	− 0.07	0.04	− 0.04	− 0.01
4	LL	$T_{7–9}$	− 0.28	0.50	− 0.11	0.30	0.18	− 0.09	− 0.10	0.03	− 0.04	− 0.66	− 0.02	− 0.24
4	LL	$T_{0–END}$	− 0.15	0.08	0.00	− 0.02	0.05	0.00	− 0.02	0.09	0.01	− 0.11	0.00	− 0.02
5	HL	$T_{0–3}$	0.17	0.21	0.08	− 0.04	− 0.09	0.25	− 0.34	0.17	0.05	− 0.28	0.08	− 0.06
5	HL	$T_{3–7}$	0.15	0.27	0.20	0.19	0.20	0.28	− 0.18	0.22	0.08	− 0.15	0.21	0.11
5	HL	$T_{7–9}$	0.12	0.23	0.16	− 0.07	0.14	0.21	0.56	0.19	0.20	0.39	0.18	0.21
5	HL	$T_{0–END}$	0.15	0.24	0.15	0.05	0.09	0.25	− 0.07	0.20	0.10	− 0.07	0.16	0.07
5	ML	$T_{0–3}$	0.07	0.28	0.11	− 0.15	− 0.04	0.21	− 0.51	0.31	0.19	0.03	0.11	0.07
5	ML	$T_{3–7}$	− 0.17	0.23	0.17	0.15	0.15	0.17	− 0.05	0.24	0.20	− 0.09	0.18	0.11
5	ML	$T_{7–9}$	0.36	0.12	0.07	− 0.05	0.15	0.28	0.60	0.12	0.10	− 0.12	0.11	0.09
5	ML	$T_{0–END}$	0.03	0.22	0.13	0.01	0.09	0.21	− 0.06	0.24	0.18	− 0.06	0.14	0.09
5	LL	$T_{0–3}$	− 0.04	− 0.13	− 0.07	− 0.07	0.01	0.04	− 0.17	0.01	− 0.19	0.17	− 0.06	0.00
5	LL	$T_{3–7}$	− 0.12	0.03	0.02	− 0.11	− 0.20	0.22	− 0.38	− 0.16	− 0.23	− 0.14	− 0.01	− 0.11
5	LL	$T_{7–9}$	0.11	− 0.09	0.00	− 0.10	0.08	0.05	0.30	0.21	0.08	0.27	0.01	0.17
5	LL	$T_{0–END}$	− 0.05	− 0.05	− 0.02	− 0.12	− 0.08	0.12	− 0.15	− 0.01	− 0.15	0.05	− 0.02	− 0.01

Table 4 (continued)

INC	Light level	Time period	Phyto I	Phyto II	Phyto III	Phyto IV	Phyto V	Phyto VI	Phyto VII	Phyto VIII	Phyto IX	Phyto X	FCM -ab	FCM -C
6	HL	$T_{0–3}$	0.25	0.16	0.13	0.10	0.20	0.03	− 0.13	0.22	− 0.16	− 0.18	0.13	0.01
6	HL	$T_{3–7}$	0.30	0.39	0.27	0.18	0.31	0.26	0.19	0.45	0.21	0.31	0.28	0.29
6	HL	$T_{7–9}$	0.11	0.26	0.17	0.22	0.53	0.59	0.81	0.16	0.48	0.13	0.25	0.27
6	HL	$T_{0–END}$	0.24	0.28	0.20	0.16	0.32	0.26	0.22	0.31	0.15	0.11	0.23	0.19
6	ML	$T_{0–3}$	0.23	0.20	0.13	0.08	0.19	0.18	0.35	0.16	0.07	0.22	0.15	0.17
6	ML	$T_{3–7}$	0.23	0.34	0.21	0.15	0.33	0.17	− 0.01	0.15	0.41	0.24	0.24	0.23
6	ML	$T_{7–9}$	0.09	0.27	0.28	0.14	0.32	0.48	0.25	0.68	− 0.26	0.16	0.29	0.25
6	ML	$T_{0–END}$	0.20	0.28	0.20	0.13	0.28	0.24	0.17	0.27	0.15	0.22	0.22	0.21
6	LL	$T_{0–3}$	0.15	− 0.06	0.07	0.09	0.02	0.01	− 0.19	− 0.10	0.11	0.13	0.05	0.08
6	LL	$T_{3–7}$	0.15	0.02	0.00	− 0.03	0.05	0.05	0.04	0.04	0.16	− 0.02	0.01	0.01
6	LL	$T_{7–9}$	0.25	0.15	0.12	− 0.04	0.15	0.26	0.07	− 0.08	0.08	0.31	0.13	0.17
6	LL	$T_{0–END}$	0.17	0.02	0.05	0.01	0.06	0.08	− 0.03	− 0.04	0.12	0.10	0.05	0.07

Accumulation rates represent an average of triplicates

maintained, both at the start ($T_{0–3}$) and overall ($T_{0–9}$; Online Resource 5 and 8), with average total abundance-based accumulation rates ranging from − 0.06 to 0.06 day^{-1} (Tables 3 and 4). This coincided with essentially unchanged silicate, nitrate and phosphate concentrations under LL (Fig. 6a–c). In contrast, the accumulation rate under LL in INC 2 was 0.26 ± 0.05 day^{-1} at the start ($n = 3$) and 0.10 ± 0.02 day^{-1} overall ($n = 3$) (Table 3), coinciding with nutrient drawdown under LL (Fig. 6). Concentrations of nitrate and phosphate were low at the start of INC 2 (Fig. 6b, c) which may have reduced the accumulation rates after the first 3 days, especially the relatively large-sized Phyto IX which dominated both flow cytometry abundance and carbon accumulation rates (0.32 ± 0.08 day^{-1}, $n = 3$; Table 3). Phosphate and nitrate concentrations were also low at the start of INC 5, yet no large reduction in total abundance-based accumulation rates was observed (Table 4), which may be due to low numbers of the larger-sized phytoplankton populations (Online Resource 8). Low nutrient concentrations could also have reduced accumulation rates towards the end of INC 3 and 4 ($T_{7–9}$) under HL and ML (Table 4).

The phytoplankton community at the end of INC 1 under ML (the light intensity most similar to the ambient light level at the start of the experiment) was highly comparable to that of the natural community sampled around that time (30–50 µmol quanta m^{-2} s^{-1}), i.e. the dominant populations Phyto III, VI and IX made up 19 ± 5, 58 ± 9 and 10 ± 1% ($n = 3$) at ML in INC1 (Online Resource 5) versus 20, 55 and 9% under natural conditions (Biggs et al. 2019). This suggests that the incubations successfully replicated natural conditions. Diatoms Phyto VI were the most abundant phytoplankton group in INC 1 (initial concentrations of 1.1 ± 0.2 × 10^3 cells mL^{-1}, $n = 8$; Fig. 2b) and grew well throughout the experiment (0.27 ± 0.03 day^{-1}, $n = 2$; Table 3). Phyto VI subsequently contributed the dominant portion of total abundance-based accumulation rates in the ML incubations (Fig. 5c). During the other experiments (INC 2–6) relatively high Phyto VI abundance accumulation rates were observed under ML as well as HL. Highest Phyto VI carbon concentrations (> 12 µg C L^{-1}) were observed during INC 1, 2 and 5 (Online Resource 6 and 9), the only incubations where temperature was > 0 °C. This is compared to INC 3, 4 and 6 where concentrations remained ≤ 7 µg C L^{-1} (Online Resource 6 and 9). This is unlike the similar sized diatom Phyto V where highest abundances were observed under HL and ML at the end of INC 3, where temperatures were lowest and in situ PAR highest (Table 2). Comparing accumulation rates of Phyto V during the first three days of all experiments, highest rates were also observed under HL and ML at the start of INC 3, with Phyto V and X displaying the largest rates of all Phyto groups (0.31 to 0.35 day^{-1}; Tables 3 and 4). Highest concentrations of the largest diatom Phyto X were observed during INC 2, 3 and

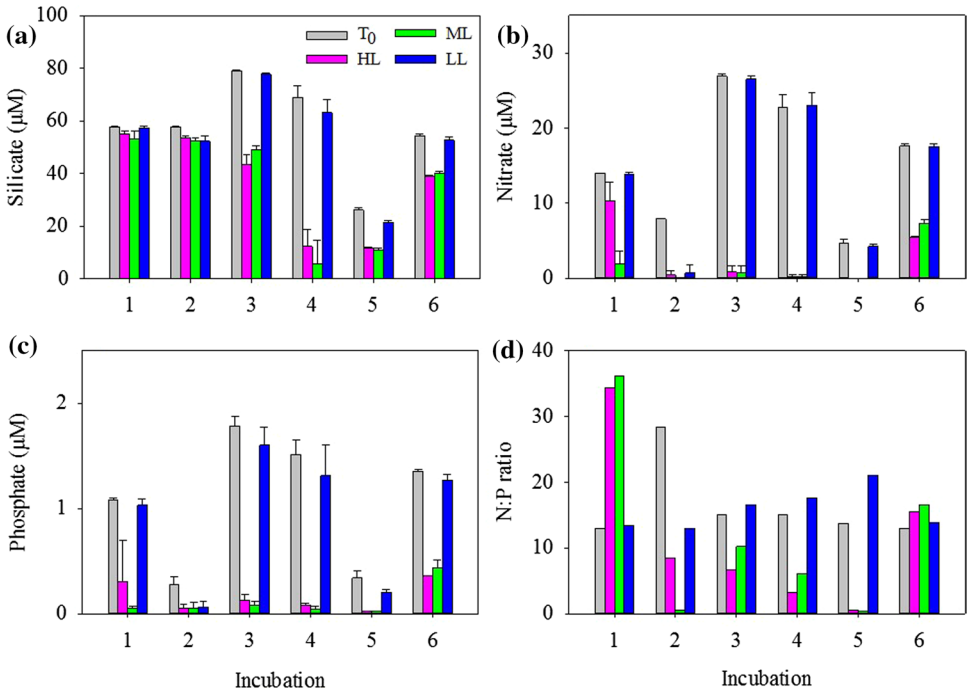

Fig. 6 Average dissolved inorganic nutrient concentrations in water used for the experimental setup (grey bar; T_0) and at termination of the experiment, for light treatments high light (HL, magenta bars), medium light (ML, green bars) and low light (LL, blue bars) for **a** silicate, **b** nitrate, **c** phosphate and **d** the average nitrate-to-phosphate ratios. Error bars represent ± 1 standard deviation whereby all time zero replicates are combined (INC 1 and 2 $n = 2$, INC 3–6 $n = 9$) and shown at the beginning of each INC and at the end under HL, ML and LL treatments

4 under HL and ML (peak abundance ≥ 680 cells mL^{-1}), compared to INC 1, 5 and 6 where numbers under HL and ML remained low throughout (< 50 cells mL^{-1}).

The diatoms Phyto IX (11.5 µm) dominated FCM-C under both ML and HL in INC 1 (439 ± 27 and 754 ± 251 µg C L^{-1} at the end of the experiment; 89 ± 0.1 and 70 ± 2% of total, $n = 2$ and 3, respectively) and were responsible for the relatively high carbon-based accumulation rates (Fig. 5d). The dynamics of diatom Chl-C under HL and ML (accumulation rates of 0.41 ± 0.01 and 0.43 ± 0.01 day^{-1} $n = 2$ and 3, respectively; Online Resource 10) were indeed similar to Phyto IX (0.48 ± 0.04 and 0.42 ± 0.02 day^{-1} $n = 2$; Table 3). Similarly, the Chl-C net growth rates of prymnesiophytes and cryptophytes under LL (0.01 ± 0.04 and − 0.04 ± 0.2 day^{-1}, $n = 3$, respectively; Online Resource 10) resembled FCM-C-based rates of *Phaeocystis* spp. Phyto III and the cryptophyte Phyto IV (− 0.08 ± 0.12 and − 0.05 ± 0.04 day^{-1}, $n = 3$, respectively; Table 3). Although abundances of *Phaeocystis* spp. Phyto III were relatively high at the end of all experiments except INC 2, highest abundances were observed in INC 5 and 6 under all light treatments (Online Resource 5 and 8). The natural dynamics of this phytoplankton group were associated with reduced salinities (Biggs et al. 2019), coinciding with lowest average salinity during the 21 days prior to T_0 of INC 5 and 6 (Table 2).

INC 2 was different to the other experiments as it was the only incubation where initial ($T_{0–3}$) accumulation rates were comparable under all light regimes (abundance-based 0.22–0.26 day^{-1} and FCM-C-based 0.31–0.36 day^{-1}, Tables 3 and 4). INC 2 was also the only incubation where the natural light intensity was less than low light, both at the start and during the 21 days prior (Table 2). At the start of this experiment, total FCM-C was dominated by Phyto IX (94 ± 2% $n = 9$), with significantly higher concentrations of Phyto IX observed at the end under LL (1670 ± 108 µg C L^{-1} $n = 3$) compared to ML and HL (1210 ± 30 and 1203 ± 166 µg C L^{-1}, respectively, $n = 3$, ANOVA: $F_{2,6} = 16$, $p = 0.004$; Online Resource 6 and 9). The accumulation rates of Phyto IX, as well as for Phyto II, III, V, VII and VIII, were higher under LL compared to HL or ML (*t* test: $T_{14} = -5.1$ and − 4.2, $p < 0.001$ and < 0.001, respectively; Table 3). Only for Phyto VI and Phyto X the accumulation rates were significantly lower under LL compared to HL or ML (*t* test: $T_5 = 3.1$ and 2.6, $p = 0.014$ and 0.026, respectively; Table 3). The large-sized diatom Phyto X (20 µm) was hardly present under LL in INC 2 but thrived under ML and HL (Online Resource 6 and 9). Phyto X together with Phyto IX (roughly equal share) drove overall accumulation rates based on FCM-C under ML and HL (Fig. 5d, Table 3). Despite the similarly high biomass of the dominant Phyto IX and Phyto X under ML and HL, total Chl-*a* concentrations under HL were lower (Fig. 4a, b; Online Resource 3) and Chl-*a*-based accumulation rates were negative (Fig. 5a, b). This suggests that the cellular Chl-*a* concentrations decreased under HL. Similarly, the lower biomass (Phyto X hardly present; Online Resource 6) but higher Chl-*a* under LL (Fig. 4), compared to ML and HL, implies photoacclimation (Online Resource 3 and 5). Indeed, when pigment concentrations were normalized to cell volume (fg $µm^{-3}$; based on flow cytometry size estimations), significantly

higher concentrations of chlorophyll-c2, fucoxanthin and chlorophyll-*a* were observed at T_{END} under LL (Table 5). This also holds for the other experiments apart from INC 6 (i.e. INC 1–5, compared to HL and ML; Wilcoxon Signed Rank Test: $Z = 3.4$, 3.4, 3.4, 3.3, 3.4, 3.4, respectively, all $p < 0.001$; Table 5). Chlorophyll-based carbon concentrations at the end of INC 6 were considerably higher than FCM-C under all light levels (Fig. 4b, d), potentially indicating a greater contribution of larger phytoplankton cells that are not analysed by flow cytometry.

Discussion

The Chl-*a* accumulation rates recorded in this study (up to 0.32 day^{-1}) accord with those previously reported for Antarctic waters (up to 0.29 day^{-1}; Hutchins et al. 2001), as are the FCM-C accumulation rates (average 0.73 day^{-1}) when compared to results from ^{14}C uptake methods (1.0 day^{-1}; Smith 1999). The combined use of flow cytometry, size fractionation and chemical taxonomy allows for improved interpretation of light-regulated phytoplankton accumulation from incubation experiments. Not only does it aid in the differentiation and identification of phytoplankton groups (Biggs et al. 2019), it also clarifies which groups were contributing most to the offset in Chl-*a* accumulation in relation to light level observed in INC 2–5 (Fig. 5).

Phytoplankton community response to light intensity

This study supports the general observation that light exerts a major control on the seasonal development of net primary productivity in highly productive Antarctic marine ecosystems (Vernet et al. 2008; Petrou and Ralph 2011; Park et al. 2017). Due to acclimation of phytoplankton pigments, the combination of flow cytometry and chemical taxonomy allowed us to more accurately assess the response of the phytoplankton community to light.

Table 5 Pigment concentrations corrected for cell volume (fg μm^{-3}) for INC 1–6

INC	Light level	Time (days)	Chl-c2	Fuco	Dd + Dt	Chl-*a*	Total
1	ALL	0	0.74	2.09	0.49	6.16	11.36
1	HL	10	0.30	1.61	0.44	3.10	5.71
1	ML	10	0.52	2.76	0.30	4.91	8.94
1	LL	10	0.80	3.38	0.33	5.66	11.50
2	ALL	0	0.51	4.00	0.25	6.06	11.14
2	HL	10	0.06	0.77	0.72	1.23	2.83
2	ML	10	0.10	0.90	0.32	1.43	2.80
2	LL	10	0.32	2.31	0.23	3.58	6.57
3	ALL	0	0.34	1.01	1.04	2.40	5.22
3	HL	9	0.89	0.78	2.81	0.11	4.74
3	ML	9	1.36	0.76	1.14	0.20	3.65
3	LL	9	2.98	7.35	1.15	10.70	23.36
4	ALL	0	1.03	2.43	0.76	2.77	7.47
4	HL	9	1.27	1.45	5.76	0.41	9.12
4	ML	9	1.01	1.57	1.32	0.60	4.65
4	LL	9	2.69	6.73	1.13	6.89	18.79
5	ALL	0	2.93	8.71	0.76	12.27	28.22
5	HL	9	0.71	1.96	2.54	2.77	8.58
5	ML	9	2.01	4.45	1.31	5.65	14.70
5	LL	9	6.43	20.12	1.75	28.13	63.67
6	ALL	0	2.68	10.13	1.89	16.24	36.60
6	HL	9	2.73	5.68	6.53	8.03	24.44
6	ML	9	8.45	22.17	5.89	19.01	61.91
6	LL	9	3.76	11.11	1.16	18.15	39.62

All time zero replicates were combined (ALL; INC 1 and 2 $n = 2$, INC 3–6 $n = 9$) as well as replicates for each light level at the end ($n = 3$). Abbreviations stand for chlorophyll-c2 (Chl-c2), fucoxanthin (Fuco), diadinoxanthin + diatoxanthin (Dd + Dt), chlorophyll-*a* (Chl-*a*) and all pigments quantified (Total), i.e. including additional pigments chlorophyll-c3, peridinine, butanoyloxyfucoxanthin, neoxanthin, prasinoxanthin, violaxanthin, hexa fucoxanthin, alloxanthin, zeaxanthin, lutein, chlorophyll-b, divinyl chlorophyll-*a*, α-caroteen and ß-caroteen

Dynamic Chl-*a* concentrations in response to different light regimes (i.e. decline under HL and strongly increase under LL) were indicative of cellular remodelling in response to shifting environmental conditions. Specifically, light-harvesting pigments were decreased when light was plentiful, whereas they were synthesized to optimize rates of photosynthesis under low-light conditions (Eppley and Sloan 1966; MacIntyre et al. 2002; Álvarez et al. 2017). Indeed, when corrected for cell volume the concentrations of Chl-*a* (as well Chl-c2 and fucoxanthin) were for all experiments (apart from INC 6) lowest under HL and highest under LL. Accumulation rates derived from Chl-*a* were thus not representative of the phytoplankton community response as indicated by shifts in FCM-C biomass. Large contributions by the large Phyto X (4413 μm^3) in INC 2–4 coincided with extremely low concentrations of Chl-*a* (cell $volume^{-1}$) at HL, implying this diatom population is able to rapidly adjust Chl-*a* concentrations in relation to light level (Finkel 2001; Álvarez et al. 2017) to optimize growth. Whilst Chl-*a* per cell volume increased under LL in INC 3–5, concentrations remained relatively unchanged in INC 1 and 6 (Table 5), coinciding with peak prasinophyte contributions and positive net growth rates for prasinophytes at all light levels (only in INC 1 and 6; Online Resource 7 and 10). Large-sized (> 20 µm diameter, Bird and Karl 1991) and mixotrophic prasinophytes, such as *Pyramimonas* spp. (Bell and Laybourn-Parry 2003), could partially explain the lack of a pigment response to light level as they would not need to adjust their photosynthetic pigment content under low-light intensity.

With the exception of INC 2, exposure to low light did not result in noteworthy accumulation, suggesting that the low-light intensity used was close to a threshold where (reduced) phytoplankton growth is equal to naturally occurring losses (Behrenfeld and Boss 2018). The slight decrease in nutrient concentrations in these incubations indicates that phytoplankton gross growth rates were likely to be positive (Biggs et al. 2020). An interesting exception to this trend was observed in INC 2 where biomass accumulation was observed under low light. Equivalent phytoplankton abundance and FCM-C-based accumulation were recorded for all three light treatments (especially during the first 3 days), implying the growth potential of the phytoplankton community used to set up INC 2 was different compared with the other experiments. For the three weeks prior to INC 2, natural PAR was very low (average 1.7 µmol quanta m^{-2} s^{-1}) which likely instigated physiological changes that allowed higher growth rates under LL but with reduced growth potential under ML and HL conditions (Dubinsky and Stambler 2009). Sloughter et al. (2019) estimated compensation intensities from the literature at 5–25 µE m^{-2} s^{-1} (Langdon 1988; Boyd et al. 1995; Quigg and Beardall 2003) with the lower end of this range similar to low-light intensity employed in our study. Venables et al. (2013) showed that phytoplankton biomass accumulation in Antarctic waters begins when average PAR rises above a threshold of ~ 1 µmol quanta m^{-2} s^{-1}. Our study suggests that at these lower light levels (1–7 µmol quanta m^{-2} s^{-1}) phytoplankton start to adjust their (light regulated) growth potential. Sloughter et al. (2019) proposed a trade-off between the initial slope (α) of the photosynthesis–irradiance (PE) curve and respiration such that below a compensation light intensity it becomes advantageous to decrease α to offset the costs of respiration. During prolonged periods of low light, such as after the winter period but also before INC 2, having a low growth potential would allow higher growth rates under low light (as compared to summer periods with increased light availability, such as INC 1 and 3–6, that allow a high growth potential to achieve maximum rates of realizable growth). These results indicate that it becomes advantageous to adjust growth potential over relatively short time periods to best utilize available light during the austral summer.

Prolonged periods of low light may also occur during natural phytoplankton blooms in this coastal environment (where Chl-*a* concentrations regularly exceed 15 µg L^{-1}; Clarke et al. 2008; Venables et al. 2013; Park et al. 2017). The extremely low-light level coinciding with the setup of INC 2 (0.3 µM quanta m^{-2} s^{-1}) likely resulted from light attenuation owing to peak density of a phytoplankton bloom. The low-light levels used in this study could thus, in addition, represent a tipping point around which growth potential is maximized, and the length of time spent above or below this threshold determines if blooms either develop or decline. The length of the photoperiod follows a seasonal pattern and shorter day length would also affect the phytoplankton community sampled later in the season. Accumulation rates for INC 6 in late February (S2) were positive under LL (0.05 ± 0.02 and 0.07 ± 0.02 day^{-1} for phytoplankton abundance and FCM-C, $n = 3$); however, light intensity was still relatively high (average 39 µmol quanta m^{-2} s^{-1}). The community may have been acclimating to lower daily PAR (Dubinsky and Stambler 2009) but still in a high growth state (Sloughter et al. 2019) due to exposure to sufficiently high-intensity PAR at mid-day, especially if coinciding with deeper vertical mixing (Alderkamp et al. 2010). Ambient light levels were low for at least six days prior to INC 4 (average of 1.2 µmol quanta m^{-2} s^{-1}) and this period probably extended to 14 days due to 90–100% ice cover (and high biomass); however, accumulation of FCM-ab and FCM-C under LL was zero. Therefore, adjustments to optimize growth potential under low light (Sloughter et al. 2019) seem to be forced by low-light exposure over a period as little as three weeks. Temperature could also be a factor as relatively high temperatures were observed prior to INC 2 (1 ± 0.2 °C, $n = 7$) compared to INC 4 and 6 (-0.5 ± 0.3 and 0 ± 0.6 °C, $n = 8$ and 7, respectively; Table 2). Relatively

higher respiration costs compared to photosynthesis at higher temperatures (Boscolo-Galazzo et al. 2018) could potentially increase the compensation light level that triggers more long-term adjustments to growth potential.

Potential losses

As untreated natural seawater was used to set up the experiments, the phytoplankton responses observed are the result of gross growth (controlled by the bottom-up growth factors such as light in our study) minus top-down loss processes (such as zooplankton grazing and viral lysis). Cell mortality due to lytic virus infection has been shown as a substantial loss factor for phytoplankton in general (Brussaard and Martínez 2008; Mojica et al. 2016). More specifically, viruses were important mortality agents for all ecologically relevant Antarctic phytoplankton groups (average of 0.29 day^{-1} in S1 and 0.22 day^{-1} in S2; Biggs et al. 2021 and unpublished data). The appearance of an algal virus-like group in INC 6 (Online Resource 11) also hints to the potential influence of viruses in our incubations. The staining characteristics of the virus we observed implies it comprised a larger genome virus akin to non-silicified phytoplankton viruses, such as those that infect *Phaeocystis* spp. (Brussaard et al. 1999; Baudoux and Brussaard 2005). The abundance of this virus cluster increased during the experiment under the ML and HL but not under the LL treatment. *Phaeocystis* spp. Phyto III was very abundant in INC 6 and net growth was on average 0.2 ± 0.01 day^{-1} ($n = 6$) at ML and HL and 0.05 ± 0.02 day^{-1} ($n = 3$) at LL. These virus and phytoplankton dynamics could imply coupling of lytic infection rates and host growth rates (Maat et al. 2017; Piedade et al. 2018; Gann et al. 2020). Such a strategy is ecologically sound as it supports persistence of the virus population throughout the growth season without decimating the host population and allowing the persistence of cells over the winter period. Hypothesizing it to be a *Phaeocystis* spp. virus and assuming no loss of viruses and the burst size to be 300 viruses per lysed host cell (Brussaard et al. 2007), about 570 cells would be lysed over the incubation period (at ML and HL). This equals ~ 10% of the standing stock of the host and relates well to the specific viral lysis rates around the starting date of INC 6 (0.16 and 0.10 day^{-1} on 17 and 27 February; unpublished data). Delayed and reduced virus production under low-light conditions have been reported for several phytoplankton species including temperate *Phaeocystis globosa* (Baudoux and Brussaard 2008; Maat et al. 2016; Piedade et al. 2018; Gann et al. 2020) as a result of photolimitation, which could explain the lack of virus production under the LL intensities employed in our study.

Besides viral lysis and microzooplankton grazing on the various phytoplankton populations (Biggs et al. 2021), larger-sized zooplankton grazing may have occurred. These larger zooplankton graze selectively on diatoms (rather than cryptophytes and prymnesiophytes, even when diatoms are rare; Nejstgaard et al. 1994; Haberman et al. 2003; Mitra et al. 2014) and larger-sized diatoms are preferred prey (Sommer and Stibor 2002; Gonçalves et al. 2014; Djeghri et al. 2018). The large diatom Phyto X was found in high abundance during INC 2–4 but at low abundances in INC 1, 5 and 6. Based on the dataset in Biggs et al. (2020), larger zooplankton were predicted to number 5–11 ind. $bottle^{-1}$ at the start of these incubations and selective zooplankton grazing may have restricted the accumulation of Phyto X in INC 1, 5 and 6. In contrast, INC 2–4 were likely subject to far less larger zooplankton-induced mortality owing to their lower predicted abundance at 2–4 ind. $bottle^{-1}$.

Phytoplankton group-specific differences

Phaeocystis spp. Phyto III typically grew best under ML and HL, but the relatively high accumulation rates under LL in INC 2 and INC 6 suggest this phytoplankton group can compete under all ecologically relevant light conditions. Light intensities during *Phaeocystis antarctica*-dominated blooms can be low (Schofield et al. 2015; Park et al. 2017; Oliver et al. 2019) and *P. antarctica* seems better suited, compared to diatoms, to a more dynamic light regime associated with deeper mixed layers (Alderkamp et al. 2010; Arrigo et al. 2010; Mills et al. 2010). Photoacclimation has been shown to effectively minimize photoinhibition in natural populations of *P. antarctica* (Alderkamp et al. 2013). Our study supports a modelling study of *P. antarctica* blooms (Amundsen Sea Polynya; Oliver et al. 2019) which suggested a high degree of photophysiological control (relative to nutrient processes) and the importance of shifts in α that dictate bloom progression under low light. The capability to adjust growth potential over relatively short time scales may contribute to its ecological success.

Studies into photoacclimation of Antarctic phytoplankton reveal that diatoms show a variable response to changes in light intensity, resulting in a high degree of specialized niche differentiation (Petrou et al. 2016). In our study, diatom Phyto IX acclimated best to low light with the highest accumulation rates of all phytoplankton groups, matching the strong association of Phyto IX with low and limiting PAR under natural conditions (Biggs et al. 2019). This could partly be explained by its intermediate cell volume (estimated as 792 μm^3), being large enough to take advantage of space requirements (by cellular machinery) for efficient resource acquisition, but small enough so that intracellular distances do not severely impact assimilation and also to minimize the package effect (Marañón 2015). Low light levels during dense phytoplankton blooms are not uncommon (Vernet et al. 2008; Park et al. 2017) and the ability to efficiently adapt to such conditions represents

a distinct advantage, allowing specific groups to be a key feature of coastal Antarctic phytoplankton blooms.

In summary, the low-light levels identified in this study (4–7 µmol quanta m^{-2} s^{-1}) could represent an important boundary where phytoplankton initiate more long-term adjustments to their growth potential, as observed in INC 2. This acclimation of (coastal) Antarctic phytoplankton growth potential over time periods as little as 3 weeks may allow phytoplankton to reduce their light compensation intensity, increase growth rates under low light and extend periods of phytoplankton accumulation (i.e. positive net growth). Some diatom groups (such as Phyto IX) seem ideally sized to outcompete others under low-light levels (for example during dense phytoplankton blooms or due to increased concentrations of suspended sediment), whilst others (such as Phyto VI and X) are more competitive under higher levels of light.

Phyto X needed longer to acclimate to LL, potentially due to its larger cell size (Marañón 2015) and related higher maintenance respiration costs (Langdon 1988; Quigg and Beardall 2003). The low Chl-*a* concentrations of Phyto X (cell volume^{-1}) could be a mechanism to reduce the package effect (Finkel 2001) and allow Phyto X to co-dominate phytoplankton biomass (together with Phyto IX). The earlier discussed enhanced losses of larger-sized diatom cells (such as Phyto X) during peak abundance of larger zooplankton may limit the accumulation of these diatoms, especially when combined with low-light conditions (i.e. < 8–30 µmol quanta m^{-2} s^{-1}).

The smaller-sized diatoms Phyto V and Phyto VI have both been associated with high light and temperature (Phyto VI more with temperature and Phyto V with light; Biggs et al. 2019). This would explain the strong growth of Phyto V when exposed to HL in the relatively warmer INC 1 and of Phyto VI at HL in the colder INC 3, 4 and 6. Nano-sized diatoms are poorly characterized yet play an important role in 'spring' blooms and carbon export (Leblanc et al. 2018). Our study indicates that in the current times of global climate change, it is highly relevant to study in more detail the responses of the different phytoplankton populations to growth-controlling factors, such as light. The combination of (pigment and flow cytometry based) analytical methods used in this study provided a more detailed, and hence improved, understanding of community changes in relation to light level. A better understanding is essential in times of global climate change as regionally specific differences will have regionally specific impacts on the flow of photosynthetically fixed carbon in these highly productive, light-driven ecosystems. Moreover, we recommend studying combined effects of light with other growth-controlling variables (such as temperature) and perform loss rate measurements on the various Antarctic phytoplankton groups.

Supplementary Information The online version contains supplementary material available at https://doi.org/10.1007/s00300-022-03094-5.

Acknowledgements We thank the British Antarctic Survey (BAS) for their logistical support and cooperation during the field campaign, as well as the carpenters and maintenance technicians who helped to build the experimental chamber. We also thank Zoi Farenzena and Dorien Verheyen for field assistance. Furthermore, we thank the reviewers (Andrew McMinn and anonymous reviewers) for their constructive comments that considerably improved the manuscript.

Author contributions CPDB had the project oversight; TEGB, CE and CPDB designed the study. TEGB performed the research, sample and statistical analysis. KRT provided funding for some of the sample analysis and PDR ran the CHEMTAX analysis. CE, KRT, MPM and DWP provided their expertise and advise. TEGB and CPDB analysed the data and wrote the paper and all authors commented on the final version.

Funding This work was part of the ANTPHIRCO project (Grant 866.10.102 awarded to C.P.D.B.) which was supported by The Netherlands Polar Programme and with financial aid from the Dutch Research Council (NWO). BAS scientific participation was funded by the UK Natural Environment Research Council via the Rothera Time Series (RaTS) programme.

Data availability Any data not supplied in the supplement, i.e. the raw data of experimental replicates, are available on reasonable request from the corresponding author.

Code availability Not applicable.

Declarations

Conflict of interest The authors declare no conflicts of interest/competing interests.

Ethical approval Not applicable.

Consent to participate Not applicable.

Consent for publication Not applicable.

References

Agirbas E, Feyzioglu AM, Kopuz U, Llewellyn CA (2015) Phytoplankton community composition in the south-eastern Black Sea determined with pigments measured by HPLC-CHEMTAX analyses and microscopy cell counts. J Mar Biol Assoc United Kingdom 95:35–52. https://doi.org/10.1017/S0025315414001040

Alderkamp AC, De Baar HJW, Visser RJW, Arrigo KR (2010) Can photoinhibition control phytoplankton abundance in deeply mixed water columns of the Southern Ocean? Limnol Oceanogr 55:1248–1264. https://doi.org/10.4319/lo.2010.55.3.1248

Alderkamp AC, Kulk G, Buma AGJ et al (2012) The effect of iron limitation on the photophysiology of *Phaeocystis antarctica* (Prymnesiophyceae) and *Fragilariopsis cylindrus* (Bacillariophyceae) under dynamic irradiance. J Phycol 48:45–59. https://doi.org/10.1111/j.1529-8817.2011.01098.x

Alderkamp A, Mills M, van Dijken G, Arrigo K (2013) Photoacclimation and non-photochemical quenching under in situ irradiance in natural phytoplankton assemblages from the Amundsen Sea, Antarctica. Mar Ecol Prog Ser 475:15–34. https://doi.org/10.3354/meps10097

Álvarez E, Nogueira E, López-Urrutia Á (2017) In vivo single-cell fluorescence and size scaling of phytoplankton chlorophyll content. Appl Environ Microbiol 83:1–16. https://doi.org/10.1128/aem.03317-16

Arrigo KR, van Dijken GL (2015) Continued increases in Arctic Ocean primary production. Prog Oceanogr 136:60–70. https://doi.org/10.1016/j.pocean.2015.05.002

Arrigo KR, Mills MM, Kropuenske LR et al (2010) Photophysiology in two major southern ocean phytoplankton taxa: Photosynthesis and growth of *Phaeocystis antarctica* and *Fragilariopsis cylindrus* under different irradiance levels. Integr Comp Biol 50:950–966. https://doi.org/10.1093/icb/icq021

Arrigo KR, van Dijken GL, Strong AL (2015) Environmental controls of marine productivity hot spots around Antarctica. J Geophys Res Ocean 120:5545–5565. https://doi.org/10.1002/2015JC010888

Atkinson A, Siegel V, Pakhomov EA, Rothery P (2004) Long-term decline in krill stock and increase in salps within the Southern Ocean. Nature 432:100–103. https://doi.org/10.1038/nature02950.1

Baudoux A-C, Brussaard CPD (2005) Characterization of different viruses infecting the marine harmful algal bloom species *Phaeocystis globosa*. Virology 341:80–90. https://doi.org/10.1016/j.virol.2005.07.002

Baudoux A-C, Brussaard CPD (2008) Influence of irradiance on virus-algal host interactions. J Phycol 44:902–908. https://doi.org/10.1111/j.1529-8817.2008.00543.x

Behrenfeld MJ (2010) Abandoning sverdrup's critical depth hypothesis on phytoplankton blooms. Ecology 91:977–989. https://doi.org/10.1890/09-1207.1

Behrenfeld MJ, Boss ES (2018) Student's tutorial on bloom hypotheses in the context of phytoplankton annual cycles. Glob Chang Biol 24:55–77. https://doi.org/10.1111/gcb.13858

Bell EM, Laybourn-Parry J (2003) Mixotrophy in the Antarctic phytoflagellate, *Pyramimonas gelidicola* (Chlorophyta: Prasinophyceae). J Phycol 39:644–649. https://doi.org/10.1046/j.1529-8817.2003.02152.x

Biggs TEG (2020) Chapter 8: Thesis Synthesis. In: Polar phytoplankton dynamics in relation to virus and zooplankton grazers. pp 255–270

Biggs TEG, Alvarez-Fernandez S, Evans C et al (2019) Antarctic phytoplankton community composition and size structure: importance of ice type and temperature as regulatory factors. Polar Biol 42:1997–2015. https://doi.org/10.1007/s00300-019-02576-3

Biggs TEG, Brussaard CPD, Evans C et al (2020) Plasticity in dormancy behaviour of *Calanoides acutus* in Antarctic coastal waters. ICES J Mar Sci 77:1738–1751. https://doi.org/10.1093/icesjms/fsaa042

Biggs TEG, Huisman J, Brussaard CPD (2021) Viral lysis modifies seasonal phytoplankton dynamics and carbon flow in the Southern Ocean. ISME J. https://doi.org/10.1038/s41396-021-01033-6

Bird DF, Karl DM (1991) Massive prasinophyte bloom in northern Gerlache Strait. Antarct J United States 26:152–154

Boscolo-Galazzo F, Crichton KA, Barker S, Pearson PN (2018) Temperature dependency of metabolic rates in the upper ocean: a positive feedback to global climate change? Glob Planet Change 170:201–212. https://doi.org/10.1016/j.gloplacha.2018.08.017

Boyd PW, Robinson C, Savidge G, Williams PJB (1995) Water column and sea-ice primary production during Austral spring in the Bellingshausen Sea. Deep Sea Res Part II Top Stud Oceanogr 42:1177–1200. https://doi.org/10.1016/0967-0645(95)00070-7

Brussaard CPD, Martínez J (2008) Algal bloom viruses. Plant Viruses 2:1–13

Brussaard CPD, Thyrhaug R, Marie D, Bratbak G (1999) Flow cytometric analyses of viral infection in two marine phytoplankton species, *Micromonas pusilla* (Prasinophyceae) and *Phaeocystis pouchetii* (Prymnesiophyceae). J Phycol 35:941–948. https://doi.org/10.1046/j.1529-8817.1999.3550941.x

Brussaard CPD, Bratbak G, Baudoux A-C, Ruardij P (2007) *Phaeocystis* and its interaction with viruses. Biogeochemistry 83:201–215. https://doi.org/10.1007/s10533-007-9096-0

Brussaard CPD, Peperzak L, Beggah S et al (2016) Immediate ecotoxicological effects of short-lived oil spills on marine biota. Nat Commun 7:1–11. https://doi.org/10.1038/ncomms11206

Clarke A, Meredith MP, Wallace MI et al (2008) Seasonal and interannual variability in temperature, chlorophyll and macronutrients in northern Marguerite Bay, Antarctica. Deep Res Part II Top Stud Oceanogr 55:1988–2006. https://doi.org/10.1016/j.dsr2.2008.04.035

Djeghri N, Atkinson A, Fileman ES et al (2018) High prey-predator size ratios and unselective feeding in copepods: a seasonal comparison of five species with contrasting feeding modes. Prog Oceanogr 165:63–74. https://doi.org/10.1016/j.pocean.2018.04.013

Dubinsky Z, Stambler N (2009) Photoacclimation processes in phytoplankton: mechanisms, consequences, and applications. Aquat Microb Ecol 56:163–176. https://doi.org/10.3354/ame01345

Ducklow H, Clarke A, Dickhut R et al (2012) The marine system of the Western Antarctic Peninsula. In: Rogers AD, Johnston NM, Murphy EJ, Clarke A (eds) Antarctic ecosystems: an extreme environment in a changing world. Blackwell Publishing Ltd, Hoboken, pp 121–159

Eppley RW, Sloan PR (1966) Growth rates of marine phytoplankton: correlation with light absorption by cell Chlorophyll *a*. Physiol Plant 19:47–59. https://doi.org/10.1111/j.1399-3054.1966.tb09073.x

Finkel ZV (2001) Light absorption and size scaling of light-limited metabolism in marine diatoms. Limnol Oceanogr 46:86–94. https://doi.org/10.4319/lo.2001.46.1.0086

Gann ER, Gainer PJ, Reynolds TB, Wilhelm SW (2020) Influence of light on the infection of *Aureococcus anophagefferens* CCMP 1984 by a "giant virus." PLoS ONE 15:e0226758. https://doi.org/10.1371/journal.pone.0226758

García-Muñoz C, Lubián LM, García CM et al (2013) A mesoscale study of phytoplankton assemblages around the South Shetland Islands (Antarctica). Polar Biol 36:1107–1123. https://doi.org/10.1007/s00300-013-1333-5

Garibotti IA, Vernet M, Kozlowski WA, Ferrario ME (2003) Composition and biomass of phytoplankton assemblages in coastal Antarctic waters: a comparison of chemotaxonomic and microscopic analyses. Mar Ecol Prog Ser 247:27–42. https://doi.org/10.3354/meps247027

Garibotti IA, Vernet MM, Ferrario ME et al (2005) Annually recurrent phytoplanktonic assemblages during summer in the seasonal ice zone west of the Antarctic Peninsula (Southern Ocean). Deep

Res Part I Oceanogr Res Pap 52:1823–1841. https://doi.org/10.1016/j.dsr.2005.05.003
Garrison DL, Gowing MM, Hughes MP et al (2000) Microbial food web structure in the Arabian Sea: a US JGOFS study. Deep Sea Res Part II Top Stud Oceanogr 47:1387–1422. https://doi.org/10.1016/S0967-0645(99)00148-4
Gonçalves RJ, Gréve HS, Couespel D, Kiørboe T (2014) Mechanisms of prey size selection in a suspension-feeding copepod, *Temora longicornis*. Mar Ecol Prog Ser 517:61–74. https://doi.org/10.3354/meps11039
Haberman KL, Quetin LB, Ross RM (2003) Diet of the Antarctic krill (*Euphausia superba* Dana). J Exp Mar Bio Ecol 283:79–95. https://doi.org/10.1016/S0022-0981(02)00466-5
Hutchins DA, Sedwick PN, DiTullio GR et al (2001) Control of phytoplankton growth by iron and silicic acid availability in the subantarctic Southern Ocean: experimental results from the SAZ Project. J Geophys Res Ocean 106:31559–31572. https://doi.org/10.1029/2000JC000333
Kim H, Ducklow HW, Abele D et al (2018) Correction to 'Inter-decadal variability of phytoplankton biomass along the coastal West Antarctic Peninsula.' Philos Trans R Soc A 376:20180170. https://doi.org/10.1098/rsta.2018.0170
Kozlowski WA, Deutschman D, Garibotti I et al (2011) An evaluation of the application of CHEMTAX to Antarctic coastal pigment data. Deep Res Part I Oceanogr Res Pap 58:350–364. https://doi.org/10.1016/j.dsr.2011.01.008
Langdon C (1988) On the causes of interspecific differences in the growth-irradiance relationship for phytoplankton. II. A general review. J Plankton Res 10:1291–1312. https://doi.org/10.1093/plankt/10.6.1291
Leblanc K, Quéguiner B, Diaz F et al (2018) Nanoplanktonic diatoms are globally overlooked but play a role in spring blooms and carbon export. Nat Commun 9:1–12. https://doi.org/10.1038/s41467-018-03376-9
Llewellyn CA, Fishwick JR, Blackford JC (2005) Phytoplankton community assemblage in the English Channel: a comparison using chlorophyll *a* derived from HPLC-CHEMTAX and carbon derived from microscopy cell counts. J Plankton Res 27:103–119. https://doi.org/10.1093/plankt/fbh158
Llort J, Lévy M, Sallée J-B, Tagliabue A (2015) Onset, intensification, and decline of phytoplankton blooms in the Southern Ocean. ICES J Mar Sci J Du Cons 72:1971–1984. https://doi.org/10.1093/icesjms/fsv053
Maat DS, de Blok R, Brussaard CPD (2016) Combined phosphorus limitation and light stress prevent viral proliferation in the phytoplankton species *Phaeocystis globosa*, but not in *Micromonas pusilla*. Front Mar Sci. https://doi.org/10.3389/fmars.2016.00160
Maat DS, Biggs TEG, Evans C et al (2017) Characterization and temperature dependence of arctic *Micromonas polaris* viruses. Viruses 9:6–9. https://doi.org/10.3390/v9060134
MacIntyre HL, Kana TM, Anning T, Geider RJ (2002) Photoacclimation of photosynthesis irradiance response curves and photosynthetic pigments in microalgae and cyanobacteria. J Phycol 38:17–38. https://doi.org/10.1046/j.1529-8817.2002.00094.x
Mackey MD, Mackey DJ, Higgins HW, Wright SW (1996) CHEMTAX—a program for estimating class abundances from chemical markers: application to HPLC measurements of phytoplankton. Mar Ecol Prog Ser 144:265–283. https://doi.org/10.3354/meps144265
Marañón E (2015) Cell size as a key determinant of phytoplankton metabolism and community structure. Ann Rev Mar Sci 7:241–264. https://doi.org/10.1146/annurev-marine-010814-015955
Marie D, Partensky F, Vaulot D, Brussaard CPD (1999) Enumeration of phytoplankton, bacteria, and viruses in marine samples. Curr Protoc Cytom. https://doi.org/10.1002/0471142956.cy1111s10
Maxwell K, Johnson GN (2000) Chlorophyll fluorescence—a practical guide. J Exp Bot 51:659–668. https://doi.org/10.1093/jexbot/51.345.659
Mendes CRB, de Souza MS, Garcia VMT et al (2012) Dynamics of phytoplankton communities during late summer around the tip of the Antarctic Peninsula. Deep Res Part I-Oceanographic Res Pap 65:1–14. https://doi.org/10.1016/j.dsr.2012.03.002
Mendes CRB, Tavano VM, Dotto TS et al (2017) New insights on the dominance of cryptophytes in Antarctic coastal waters: a case study in Gerlache Strait. Deep Sea Res Part II Top Stud Oceanogr 149:161–170. https://doi.org/10.1016/j.dsr2.2017.02.010
Meredith MP, Renfrew IA, Clarke A et al (2004) Impact of the 1997/98 ENSO on upper ocean characteristics in Marguerite Bay, western Antarctic Peninsula. J Geophys Res C Ocean 109:1–19. https://doi.org/10.1029/2003JC001784
Meredith M, Sommerkorn M, Cassotta S et al (2022) Polar regions. In: Pörtner H-O, Roberts DC, Masson-Delmotte V et al (eds) The ocean and cryosphere in a changing climate. Cambridge University Press, Cambridge, pp 203–320
Mills MM, Kropuenske LR, Van Dijken GL et al (2010) Photophysiology in two Southern Ocean phytoplankton taxa: Photosynthesis of *Phaeocystis antarctica* (Prymnesiophyceae) and *Fragilariopsis cylindrus* (Bacillariophyceae) under simulated mixed-layer irradiance. J Phycol 46:1114–1127. https://doi.org/10.1111/j.1529-8817.2010.00923.x
Mitra A, Castellani C, Gentleman WC et al (2014) Bridging the gap between marine biogeochemical and fisheries sciences; configuring the zooplankton link. Prog Oceanogr 129:176–199. https://doi.org/10.1016/j.pocean.2014.04.025
Mojica KDA, Huisman J, Wilhelm SW, Brussaard CPD (2016) Latitudinal variation in virus-induced mortality of phytoplankton across the North Atlantic Ocean. ISME J 10:500–513. https://doi.org/10.1038/ismej.2015.130
Montes-Hugo M, Doney SC, Ducklow HW et al (2009) Recent changes in phytoplankton communities associated with rapid regional climate change along the western Antarctic Peninsula. Science (80-) 323:1470–1473. https://doi.org/10.1126/science.1164533
Moore CM, Suggett DJ, Hickman AE et al (2006) Phytoplankton photoacclimation and photoadaptation in response to environmental gradients in a shelf sea. Limnol Oceanogr 51:936–949. https://doi.org/10.4319/lo.2006.51.2.0936
Nejstgaard JC, Witte HJ, van der Wal P, Jacobsen A (1994) Copepod grazing during a mesocosm study of an *Emiliania huxleyi* (Prymnesiophyceae) bloom. Sarsia 79:369–377. https://doi.org/10.1080/00364827.1994.10413568
Oliver H, St-Laurent P, Sherrell RM, Yager PL (2019) Modeling iron and light controls on the summer *Phaeocystis antarctica* bloom in the Amundsen Sea Polynya. Global Biogeochem Cycles 2018GB006168. https://doi.org/10.1029/2018GB006168
Park J, Kuzminov FI, Bailleul B et al (2017) Light availability rather than Fe controls the magnitude of massive phytoplankton bloom in the Amundsen Sea polynyas, Antarctica. Limnol Oceanogr 62:2260–2276. https://doi.org/10.1002/lno.10565
Petrou K, Ralph PJ (2011) Photosynthesis and net primary productivity in three Antarctic diatoms: possible significance for their distribution in the Antarctic marine ecosystem. Mar Ecol Prog Ser 437:27–40. https://doi.org/10.3354/meps09291
Petrou K, Kranz SA, Trimborn S et al (2016) Southern Ocean phytoplankton physiology in a changing climate. J Plant Physiol 203:135–150. https://doi.org/10.1016/j.jplph.2016.05.004
Piedade GJ, Wesdorp EM, Montenegro-Borbolla E et al (2018) Influence of irradiance and temperature on the virus MpoV-45T infecting the Arctic picophytoplankter *Micromonas polaris*. Viruses 10:676. https://doi.org/10.3390/v10120676
Quigg A, Beardall J (2003) Protein turnover in relation to maintenance metabolism at low photon flux in two marine microalgae. Plant

Cell Environ 26:693–703. https://doi.org/10.1046/j.1365-3040.2003.01004.x
Rembauville M, Blain S, Caparros J, Salter I (2016) Particulate matter stoichiometry driven by microplankton community structure in summer in the Indian sector of the Southern Ocean. Limnol Oceanogr 61:1301–1321. https://doi.org/10.1002/lno.10291
Rozema PD, Kulk G, Veldhuis MP et al (2017a) Assessing drivers of coastal primary production in northern Marguerite Bay, Antarctica. Front Mar Sci 4:1–20. https://doi.org/10.3389/fmars.2017.00184
Rozema PD, Venables HJ, van de Poll WH et al (2017b) Interannual variability in phytoplankton biomass and species composition in northern Marguerite Bay (West Antarctic Peninsula) is governed by both winter sea ice cover and summer stratification. Limnol Oceanogr 62:235–252. https://doi.org/10.1002/lno.10391
Schofield O, Miles T, Alderkamp AC, et al (2015) In situ phytoplankton distributions in the Amundsen Sea Polynya measured by autonomous gliders. Elem Sci Anthr 3:000073. https://doi.org/10.12952/journal.elementa.000073
Sloughter TM, Banas NS, Sambrotto RN (2019) Seasonal variation in light response of polar phytoplankton. J Mar Syst 191:64–75. https://doi.org/10.1016/j.jmarsys.2018.12.003
Smith W (1999) Phytoplankton growth rates in the Ross Sea, Antarctica, determined by independent methods: temporal variations. J Plankton Res 21:1519–1536. https://doi.org/10.1093/plankt/21.8.1519
Sommer U, Stibor H (2002) Copepoda - Cladocera - Tunicata: the role of three major mesozooplankton groups in pelagic food webs. Ecol Res 17:161–174. https://doi.org/10.1046/j.1440-1703.2002.00476.x
Stammerjohn SE, Martinson DG, Smith RC et al (2008) Trends in Antarctic annual sea ice retreat and advance and their relation to El Niño-Southern Oscillation and Southern Annular Mode variability. J Geophys Res 113:C03S90. https://doi.org/10.1029/2007JC004269
Strzepek RF, Boyd PW, Sunda WG (2019) Photosynthetic adaptation to low iron, light, and temperature in Southern Ocean phytoplankton. Proc Natl Acad Sci USA 116:4388–4393. https://doi.org/10.1073/pnas.1810886116
Taylor MH, Losch M, Bracher A (2013) On the drivers of phytoplankton blooms in the Antarctic marginal ice zone: a modeling approach. J Geophys Res Ocean 118:63–75. https://doi.org/10.1029/2012JC008418
Thomalla SJ, Fauchereau N, Swart S, Monteiro PMS (2011) Regional scale characteristics of the seasonal cycle of chlorophyll in the Southern Ocean. Biogeosciences 8:2849–2866. https://doi.org/10.5194/bg-8-2849-2011
Timmermans KR, Davey MS, Van der Wagt B et al (2001) Co-limitation by iron and light of *Chaetoceros brevis, C. dichaeta and C. calcitrans* (Bacillariophyceae). Mar Ecol Prog Ser 217:287–297. https://doi.org/10.3354/meps217287
van Leeuwe MA, Webb AL, Venables HJ et al (2020) Annual patterns in phytoplankton phenology in Antarctic coastal waters explained by environmental drivers. Limnol Oceanogr 65:1651–1668. https://doi.org/10.1002/lno.11477
Venables H, Moore CM (2010) Phytoplankton and light limitation in the Southern Ocean: learning from high-nutrient, high-chlorophyll areas. J Geophys Res 115:C02015. https://doi.org/10.1029/2009JC005361
Venables HJ, Clarke A, Meredith MP (2013) Wintertime controls on summer stratification and productivity at the western Antarctic Peninsula. Limnol Oceanogr 58:1035–1047. https://doi.org/10.4319/lo.2013.58.3.1035
Vernet M, Martinson D, Iannuzzi R et al (2008) Primary production within the sea-ice zone west of the Antarctic Peninsula: I—Sea ice, summer mixed layer, and irradiance. Deep Sea Res Part II Top Stud Oceanogr 55:2068–2085. https://doi.org/10.1016/j.dsr2.2008.05.021
Winder M, Sommer U (2012) Phytoplankton response to a changing climate. Hydrobiologia 698:5–16. https://doi.org/10.1007/s10750-012-1149-2
Worden AZ, Nolan JK, Palenik B (2004) Assessing the dynamics and ecology of marine picophytoplankton: the importance of the eukaryotic component. Limnol Oceanogr 49:168–179. https://doi.org/10.4319/lo.2004.49.1.0168
Wright SW, Van den Enden RL (2000) Phytoplankton community structure and stocks in the East Antarctic marginal ice zone (BROKE survey, January-March 1996) determined by CHEMTAX analysis of HPLC pigment signatures. Deep Res Part II Top Stud Oceanogr 47:2363–2400. https://doi.org/10.1016/S0967-0645(00)00029-1
Wright SW, van den Enden RL, Pearce I et al (2010) Phytoplankton community structure and stocks in the Southern Ocean (30–80°E) determined by CHEMTAX analysis of HPLC pigment signatures. Deep Sea Res Part II Top Stud Oceanogr 57:758–778. https://doi.org/10.1016/j.dsr2.2009.06.015